Docusign Envelope ID: 7E4C2DFC-1112-4D5D-8C31-F4048EAE7E40

Title: Enhanced muscle uptake of chemically optimized miR-23b antisense oligonucleotides as lead compounds for Myotonic Dystrophy type 1

Authors: Irene González-Martínez[1,2,3,#], Estefanía Cerro-Herreros[1,2,#†], Marc Carrascosa-Sàez[4,‡], Andrea García-Rey[1,2] , Diego Piqueras Losilla[4] Anna Colom-Rodrigo[4,§] Nerea Moreno[1,2,3], Mouli Chakraborty[4], Aline Huguet-Lachon[5,] Anchel González-Barriga[5], Neia Naldaiz-Gastesi[6,7,8], Martxel Dehesa[6,7,8], Nuria Barquero[4], Miguel A Varela[9,10], Adolfo López de Munain[6,7,8,11,12], Ramon Eritja[13,14], Geneviève Gourdon[5], Arturo López-Castel[1,2,3], Manuel Pérez-Alonso[1,2,3],Beatriz Llamusi[4], and Rubén Artero[1,2,3*]

Affiliations:

[1] Human Translational Genomics Group, University Institute for Biotechnology and Biomedicine (BIOTECMED), University of Valencia; Valencia, Spain.
[2] INCLIVA Biomedical Research Institute; Valencia, Spain.
[3] CIBERER, IISCIII; Madrid, Spain.
[4]ARTHEx Biotech, Centro de Investigación Príncipe Felipe (CIPF); Valencia, Spain.
[5]Sorbonne Université, Inserm, Institut de Myologie, Centre de Recherche en Myologie; Paris, France.
[6] Biodonostia-BioGipuzkoa, Neurosciences Area, Neuromuscular Diseases Laboratory; San Sebastian, Spain.
[7] Department of Neurology, Hospital Universitario Donostia. OSAKIDETZA, San Sebastian, Spain.
[8] CIBERNED, ISCIII; Madrid, Spain.
[9] Department of Paediatrics, Institute of Developmental and Regenerative Medicine (IDRM), University of Oxford; Oxford, UK.
[10] MDUK Oxford Neuromuscular Centre, University of Oxford; Oxford, UK.
[11] Department of Neurosciences, University of the Basque Country, San Sebastian, Spain.
[12] Faculty of Health Sciences, University of Deusto, Bilbao, Spain.
[13] Nucleic Acids Chemistry Group, Institute for Advanced Chemistry of Catalonia (IQAC-CSIC), Barcelona, Spain.
[14] Networking Center on Bioengineering, Biomaterials and Nanomedicine (CIBER-BBN), Barcelona, Spain.

[#] Contributed equally.

*Corresponding author. Email: ruben.artero@uv.es

† Present address: ARTHEx Biotech, Scientific Park, Universitat de València; Paterna, Valencia, Spain.

‡ Present address: Institute for Integrative Systems Biology (I2SysBio), Consejo Superior de Investigaciones Científicas, Universitat de València; Paterna, Valencia, Spain.

§ Present address: Human Translational Genomics Group, University Institute of Biotechnology and Biomedicine (BIOTECMED), Universitat de València; Burjasot, Spain.

One Sentence Summary: Conjugation to oleic acid and chemical optimization improved muscle uptake and therapeutic potential of antimiR-23b oligos

Docusign Envelope ID: 7E4C2DFC-1112-4D5D-8C31-F4048EAE7E40

Abstract:

We developed chemically optimized antisense oligonucleotides (antimiRs) targeting miR-23b, a microRNA overexpressed in myotonic dystrophy type 1 (DM1), a multisystemic genetic disorder caused by CTG repeat expansions in the *DMPK* gene. This pathological expansion triggers an RNA sequestration mechanism, where mutant transcripts form ribonuclear foci that bind and deplete MBNL. Combined with miR-23b-mediated repression, these events exacerbate splicing defects and downstream cellular dysfunction. Our approach aimed to restore functional MBNL1 protein levels by antagonizing miR-23b effects. Using a multi-step screening process, we evaluated antimiRs with varied sequences, lengths, chemical modifications, and lipid conjugations. A critical optimization was the inclusion of a 3'-end oleic acid conjugation, together with a specific chemical pattern of modifications, which significantly enhanced the muscle uptake and efficacy of lead candidates, demonstrated robust biological activity in preclinical models, including HSA^{LR} and DMSXL mice, and human primary myoblasts. Lead candidates significantly increased MBNL1 protein levels, corrected mis-splicing events, improved functional outcomes such as muscle strength and reduced myotonia, and exhibited efficient *in vivo* biodistribution to skeletal muscle, addressing a key target tissue of DM1 pathology. Toxicological assessments in vitro revealed a favorable safety profile with minimal immune activation or renal toxicity at preclinical doses. Conservation of the mechanism of action for antimiR inhibition was confirmed in rat and pig fibroblasts. Together, these findings established two lead antimiRs as promising therapeutic candidates for DM1, with improved pharmacokinetic properties, tissue targeting, and safety, and highlight the potential of miRNA-based therapies to address critical molecular defects in the genetic disorder, DM1.

Docusign Envelope ID: 7E4C2DFC-1112-4D5D-8C31-F4048EAE7E40

Main Text:

INTRODUCTION

Myotonic dystrophy type 1 (DM1) is a rare genetic disorder with an overall prevalence of 1/3,000-1/8,000 individuals worldwide *(1)*. Expansion of an unstable CTG microsatellite repeat in the 3'-untranslated region (UTR) of the *DM1 protein kinase* (*DMPK*) gene characterizes DM1 *(2)*. Due to errors in DNA replication and repair mechanisms, these repeats can expand during genetic transmissions, a phenomenon known as genetic anticipation, leading to earlier onset and more severe symptoms in successive generations. The length of the CTG repeat broadly correlates with disease severity, but somatic and germline instability, as well as non-CTG interruptions in expanded alleles, contribute to the variable clinical presentation of DM1 *(3)*. Skeletal muscle alterations, including muscle atrophy and myotonia, cause disabling symptoms. Muscle atrophy leads to progressive weakness, especially in distal muscles, impairing mobility and dexterity. Myotonia, characterized by delayed muscle relaxation, causes stiffness and difficulty with gripping or walking, further limiting physical function and independence *(1)*. DM1 patients suffer from multisystem clinically relevant manifestations. In the cardiac muscles, arrhythmias and conduction defects may lead to sudden cardiac death. Progressive heart muscle degeneration, marked by fibrosis and fatty infiltration, impairs systolic and diastolic function *(4)*. The smooth muscles in the gastrointestinal tract are also impacted, leading to symptoms such as dysphagia, constipation, and other digestive issues *(5)*. Additionally, respiratory muscles are weakened, contributing to breathing difficulties and increasing the risk of respiratory failure *(6)*. Central nervous system effects cause features such as hypersomnia, behavioral autism spectrum disorder, and cognitive deficits *(7, 8)*. Despite several ongoing drug development programs *(9)*, no specific drug has obtained regulatory approval for DM1 patients in any jurisdiction.

Docusign Envelope ID: 7E4C2DFC-1112-4D5D-8C31-F4048EAE7E40

Mutant *DMPK* transcripts accumulate in the nucleus and induce toxicity by affecting RNA processing mechanisms, disturbing downstream regulation of gene expression *(10)*. One key molecular event contributing to DM1 pathogenesis involves the sequestration of the Muscleblind-like splicing regulator (MBNL1 and 2) family of proteins by CUG expansions, particularly MBNL1 in skeletal muscles, forming ribonuclear aggregates, the so-called foci *(11)*. This anomalous functional depletion of MBNLs severely affects the available levels of MBNL factors, impairing their critical regulatory role in alternative pre-mRNA splicing, microRNA biogenesis, and polyadenylation *(12–14)*. Additional stress responses caused by the accumulation of toxic *DMPK* mRNA leads to the activation of MBNL1 antagonists, such as CELF1 *(15)*. Together, MBNL1 and CELF1 proteins function as developmental switches, and their imbalance in DM1 causes abnormal persistence of fetal patterns of processed mRNAs, resulting in inadequate protein isoforms or altered levels of gene expression *(16)*. This pathological mechanism affects hundreds of genes in various tissues and organs, many of which have been directly linked to the specific symptoms of DM1 *(17–20)*. Several reports, however, support that lack of MBNL1 function contributes the most to muscular and cognitive DM1 phenotypes *(21–27)*. This is a particularly favorable situation from a therapeutic perspective because the limited availability of MBNL1 and MBNL2 proteins, which are partially functionally redundant in the muscles *(28)*, can be compensated by upregulating *MBNL1* and/or *MBNL2* genes, which remain normal at the genomic level in patients. Indeed, MBNL1 overexpression effectively rescues DM1 phenotypes in preclinical models *(29–31)* and is well tolerated in transgenic mice *(25)*.

Recent findings indicate that miR-218 and miR-23b, translational repressors of MBNL1 and 2 *(32, 33)*, are significantly overexpressed in diseased muscle *(33, 34)*, exacerbating functional protein

Docusign Envelope ID: 7E4C2DFC-1112-4D5D-8C31-F4048EAE7E40

depletion by sequestration. Elevated miRNA levels explain the observed downregulation of MBNL1 in DM1 cell models, including primary myoblasts differentiated *in vitro (35)* and antagonizing these miRNAs with antimiRs increased MBNL1 protein expression and reduced *DMPK* in human DM1 cells *(35)*.

AntimiRs' synthetic strands of nucleic acids are designed to bind to specific miRNA molecules, thereby modulating downstream gene expression with precision. Despite many closely related splice-switching oligonucleotides and gapmers having reached clinical trials *(36)*, no antimiR is currently in medical practice. Advances in the medicinal chemistry of nucleic acids have been enormous and have occurred rapidly, aiming to improve their pharmacokinetic (PK) and pharmacodynamic (PD) properties *(37)*. For instance, nuclease resistance and enhanced plasma protein binding (leading to reduced clearance) are markedly improved by substituting the natural phosphodiester inter-nucleotide bonds with phosphorothioate (PS) linkages or incorporating locked nucleic acids (LNAs) *(38, 39)*. Similarly, some of these features are also achieved by using nucleotides with pentose modifications, including various 2'-modified sugars such as 2'-O-methyl (2'-O-Me), 2'-O-methoxyethyl (2'-MOE), and 2′-fluoro (2'-F) modifications *(37, 40)*. However, incorporating some of these modifications into candidate antisense oligonucleotide (ON) drugs can result in toxic accumulation in the liver and kidneys due to nonspecific interactions of the ON backbone with proteins, contributing to some degree of hepatic and renal damage *(41–43)*. Moreover, antisense ON uptake by some tissues and cell types is poor, with skeletal muscles being one of the most challenging, as shown in patients with the first ON that reached clinical trials in DM1 *(44, 45)*. One active research approach to solve these issues is to conjugate the ON to an antibody *(46)* or fragment of antibody for cell receptor recognition or to conjugate to small

Docusign Envelope ID: 7E4C2DFC-1112-4D5D-8C31-F4048EAE7E40

biomolecules that can influence the biodistribution of the molecule or its half-life *in vivo (47–49)*. Therapeutic ONs represent a rapidly developing and expanding therapeutic platform for treating neuromuscular and other disorders, resulting in nearly twenty approved ON-based therapies *(37, 50, 51)* for a variety of conditions, though none yet for DM1.

We report a streamlined approach to developing the proof-of-concept antimiR-23b hit *(32, 52, 53)* into lead drugs for human use, by addressing chemical optimization and ON conjugation in parallel, significantly saving time and resources. Using the Therapeutic index (Tindex) to prioritize candidates with the greatest therapeutic window, alongside established nucleic acid medicine knowledge *(54)*, top *in vitro* candidates underwent *in vivo* evaluation for dose-responsiveness, duration of activity, toxicity, immune activation, and organ biodistribution, and the mechanism of action was confirmed in rat and pig fibroblasts. These identified antimiR drugs, X82107 and X82108, showed remarkable efficacy at low doses (3 mg/kg and 6 mg/kg), in the HSA^{LR} model, increasing MBNL1 levels, correcting mis-splicing, and improving grip strength and myotonia. Oleic acid conjugation enhanced biodistribution, further alleviating DM1 symptoms without toxicity, offering a novel pathway for antimiR drug development.

RESULTS

In vitro screening of antimiR-23b ON

Looking for the most effective and safe antimiR-23b, we performed *in vitro* screenings in DM1 fibroblasts transdifferentiated into myotubes (TDMs). The first screening addressed specific miR-23b-targeting sequences, length, and chemical modifications. In TDMs transfected with each of

Docusign Envelope ID: 7E4C2DFC-1112-4D5D-8C31-F4048EAE7E40

the candidate antimiR variants, we established the T_{index} as E_{max}* (TC_{50}/EC_{50}), which integrates the maximum activity (E_{max}), median toxic concentration (TC_{50}), and median effective concentration (EC_{50}) into a single metric. EC_{50} and E_{max} values were obtained through a Quantitative Dot Blot assay *(55)* for MBNL1 protein quantification to measure antimiR activity, and TC_{50} was determined using an MTT/MTS toxicity assay. In all cases, we included for comparison purposes the antimiR-23b molecule used in our previous proof-of-concept studies, here called X820 *(34, 52)*, with the sequence 5'-GGUAAUCCCUGGCAAUGUGAU-3', 2'-OMe chemistry, PS linkages at end-proximal nucleotides, and conjugated to cholesterol at the 3' end, and its unconjugated version (X82--).

A panel of 21 unconjugated antimiR-23b molecules containing distinct sequence and chemistry variants were synthesized, and tested for their T_{index} *in vitro* (Fig. 1A,B and Supp Table 1). The results identified X821 as the most promising antimiR-23b candidate, with a T_{index} of 4018.3. This ON demonstrated a 423-fold improvement compared to X82-- (T_{index}: 9.5), our unconjugated benchmark, and a 5.9-fold improvement over the second-ranked X822 (T_{index}: 686.7). X821 exhibited the best toxicity profile *in vitro*, requiring around 16 times higher concentration than X820 to reach TC_{50} (Fig. 1B and Supp Table 1). Comparing unconjugated versions among themselves, 18 of the 21 antimiRs evaluated had a T_{index} higher than X82--, while 3 worsened the parameter.

Effects of X821 in MBNL1 levels, alternative splicing, and functional muscle defects in two DM1 mouse models

Docusign Envelope ID: 7E4C2DFC-1112-4D5D-8C31-F4048EAE7E40

Prospective lead X821 was evaluated *in vivo* subcutaneously (s.c.) to assess its therapeutic activity in a very well stablished adult-onset DM1 murine model, the *HSA*^{LR} mouse.. Additionally, we examined the effectiveness of the antimiR approach in the DMSXL mouse model, which provides a contrast to the muscle-specific *HSA*^{LR} model, and allows testing the antimiR effects in a long tract of repeats inside the human DMPK genetic environment. These complementary models allow for a comprehensive evaluation of the therapeutic efficacy of X821.

In the *HSA*^{LR} mouse, treatment with 100 mg/kg of X821 significantly increased MBNL1 protein levels in muscle without altering blood parameters (Fig. S1A,B). It also rescued *Nfix* ex 7, *Atp2a1* ex 22, and *Clcn1* ex 7a mis-splicings in both gastrocnemius (gt) and quadriceps (qd) muscles (Fig. 1C,D, S1C,D), which ultimately led to a significant reduction in myotonia grade and an increase in grip strength in treated mice (Fig. 1E). In the DMSXL mouse, X821 also increased MBNL1 protein levels in the tibialis anterior (TA) and gt muscles and rescued *Numa1* exon 16 inclusion *(56)* in TA (Fig. 1F,G). Molecular rescues were sufficient to produce a significant functional improvement in grip strength in the rear legs 2 weeks after the last injection (Fig. 1H). Taken together, these findings demonstrate that X821 effectively addressed key molecular defects, such as MBNL1 protein upregulation and alternative splicing correction in both mice, while also improving functional outcomes related to myotonia and muscle strength. Despite X821 effectively targeting miR-23b, the effects observed on muscle function were not greater than those achieved with X820 at a lower concentration *(52)*. This lack of correlation between *in vitro* and *in vivo* activity underscored the need for subsequent optimization of X821 to enhance its therapeutic potential.

Docusign Envelope ID: 7E4C2DFC-1112-4D5D-8C31-F4048EAE7E40

In vitro screening of lipidic conjugates to improve the therapeutic index

A second *in vitro* screening addressed conjugation to various moieties to improve potency and PK properties *(57, 58)*. The conjugation of hydrophobic molecules to antisense ON and their transport from blood to tissue via various strategies might be a way to improve the transport of the ON from blood to muscle tissues, leading to enhanced biodistribution and functional uptake in muscle cells *(59, 60)*, Fatty acid conjugation had never been attempted with anti-miR-type molecules but was tested here to assess the potential effects of various ligands. Thus, additional antimiR molecules were generated by synthetically conjugating different hydrophobic moieties (Fig. 2A,B, and supplemental Table 2). To isolate the impact of the moiety, the nucleotide sequence was kept identical to the original X82--, and experiments included this unconjugated version. In this screening evaluating conjugates in the 5´ end of the ONs, oleic acid (oleyl moiety; Ol) conjugation ranked first (X8200; T_{index}= 1101.4), followed by the linoleyl-antimiR (X8201; T_{index}= 400.9), which were the two conjugates with the highest ability to reduce cell toxicity (Fig. 2B). They showed a 16.10 and 5.84-fold superiority to the original X820 hit, and 155.13 and 56.35-fold enhancement to the naked version of the antimiR, respectively. Other lipid conjugations also improved T_{index} compared to the unconjugated benchmark X82-- (tocopherol, X8202; cholesterol, X8203), while conjugation to palmitic, elaidic, and stearic acids was similar or lower in terms of T_{index}.

In vivo screening of antimiR lead candidates

We hypothesized that the positive impact of Ol on T_{index} could enhance the high-performance of antimiR X821, aiming for synergistic or additive effects. Two X821 variants (X821-7 and X821-8) were designed retaining the same sequence, but including known chemical modifications to improve *in vivo* druggability, such as methylated cytosines designed to enhance stability

Docusign Envelope ID: 7E4C2DFC-1112-4D5D-8C31-F4048EAE7E40

(Supplemental Table 3), improve RNA target interaction, and reduce immunogenicity *in vivo (61)*. Both X821 variants differed only slightly in terms of LNA/MOE content, with X821-8 having higher Tm than X821-7. X821-7 served as a benchmark to evaluate the effect of Ol conjugation position on *in vivo* rescue performance in HSA^{LR} mice. The therapeutic potential was assessed by comparing the rescue of key DM1 molecular and functional parameters after a single low-dose (3 mg/kg) i.v. injection of unconjugated X821-7 or ON with Ol at the 5´ (5´X82107) or 3´ (X82107) ends (Fig. 2C).

Five days after the injection, analysis of muscle tissue revealed that both X82107 conjugate variants consistently increased MBNL1 protein levels by 1.5-fold compared to untreated animals, while unconjugated X821-7 did not (Fig. 2D). For X82107, this translated into a significant rise in the percentage of overall splicing rescue (PSR; Fig. 2E and S2A), generated from a selected panel of four mis-spliced genes in this model (*Atp2a1*, *Clcn1*, *Nfix*, and *Mbnl1*). Increases at the *Mbnl1* and 2 mRNA level were significant and similar for all three antimiR variants, whereas reduction in detected miR-23b was robust for X82107 (Fig. S2B-D). ELISA determinations revealed that the oleic-conjugated antimiR X82107 achieved higher concentrations in the skeletal muscles, which are tissues relatively resistant to ON uptake, compared to the unconjugated version (Fig. 2F). Functionally, normalized muscle strength improved significantly and similarly for all three antimiR variants, while myotonia reduction was higher for X82107 (Fig. S2E-G). Taken together, the Ol-conjugated versions at either end of the molecule were more effective than the unconjugated version.

Similar to X821-7, we generated unconjugated X821-8, featuring a different set of chemical modifications (Supplemental Table 3) and contrasted the effects of Ol (X82108) and palmitoyl

Docusign Envelope ID: 7E4C2DFC-1112-4D5D-8C31-F4048EAE7E40

(Pal) (X82148)-conjugation at the 3´-end of the molecule (Fig. 3A), using palmitoyl as a benchmark conjugate as it has been reported as an effective enhancer of ON effects in muscle *(59)*. AntimiRs were administered as before, and similarly to what had been observed with X821-7, both X82108 and X82148 conjugates outperformed the unconjugated version, andin comparison to Pal, the Ol moiety notably increased MBNL1 protein levels, significantly improving overall PSR in skeletal muscles (Fig. 3B,C; S3A). The increase at the *Mbnl1* mRNA level and reduction in detected miR-23b were significant and similar for all three X82108 variants, whereas *Mbnl2* transcript levels significantly increased only after X82108 treatment (Fig. S3B-D). Accordingly, ELISA determinations revealed that X82108 achieved higher concentrations in the skeletal muscle than the unconjugated version (Fig. 3D). Functionally, X82108-treated mice showed a significant increase in normalized strength and a robust reduction in myotonia grade, which went from 3 to less than 1 (Fig. S3E-G). Overall, from these *in vivo* experiments, X82108 and X82107 were selected as new prospective lead candidates for further assessment of preclinical features.

Boosting PD and therapeutic potential of antimiRs via oleic acid conjugation

Previous results support that Ol-conjugation improves the PD and therapeutic impact of the antimiR candidates X82107 and X82108 *in vivo*. We hypothesized that these benefits could be sequence independent and would also apply to other anitimiRs. To test this hypothesis we designed miR-218 antimiRs, as this miRNA had previously been shown to upregulate MBNL1 in human cells and mouse models and could also have therapeutic potential in DM *(32, 34, 35)*. This assessment involved a five-day treatment of HSA^{LR} mice with 3 mg/kg of an Ol-conjugated variant (X83104) compared to the unconjugated antimiR-218 control (X831-4) with an identical chemical structure (Fig. 4A,B). The spider graphs in Fig. 4C illustrate that Ol-conjugated antimiRs against

Docusign Envelope ID: 7E4C2DFC-1112-4D5D-8C31-F4048EAE7E40

miR-23b or miR-218 consistently outperformed their unconjugated counterparts across all evaluated parameters (data from FVB control mice are included in Supplemental dataset 1). These conjugates showed greater efficiency in reducing target miRNA levels, indicating enhanced molecular targeting. Additionally, treatment with the conjugated antimiRs resulted in a significant increase in MBNL1 protein levels and *Mbnl1/2* transcript expression, underscoring their ability to restore critical molecular markers associated with DM1. Splicing recovery, including improved *Mbnl1* exon 5 inclusion, was notably higher in mice treated with the conjugates, and conjugated variants also provided the most robust recovery of functional parameters, suggesting that the Ol modification enhances therapeutic potential. The overall performance of conjugated antimiRs highlights the advantages of Ol conjugation for improving molecular and functional outcomes in this disease model.

Sustained therapeutic effects of conjugated oligos

To build on the results obtained for prospective lead candidates X82107 and X82108 from the 5-day single-dose experiments, we tested the duration of activity of these 3´Ol-conjugated molecules after the same 3 mg/kg i.v. dose by evaluating tissue response at 5, 7, and 15 days post-injection (Fig. 5A, Supplemental dataset 1). Throughout the study period, both antimiRs exhibited a sustained increase in Mbnl1 protein levels compared to PBS-injected controls, with the peak effect observed five days post-treatment (Fig. 5B). Notably, X82108 consistently outperformed X82107 in this parameter at each time point. These findings are consistent with a significant overall PSR on days 5 and 7, during which protein levels were still substantially higher than in disease controls, and X82108 provided notably better splicing rescue than X82107 (Fig. 5C, Supplemental dataset 1). Both antimiRs demonstrated a comparable peak in normalized grip strength at 5 and 7 days

Docusign Envelope ID: 7E4C2DFC-1112-4D5D-8C31-F4048EAE7E40

post-injection, nearing normal values before declining to PBS-injected levels by day 15. In the context of myotonia, X82108 achieved a greater reduction than X82107 at day 5, with both converging at later time points (Fig. 5D,E, Supplemental dataset 1). Taken together, these results suggest that the activity duration for both leads ranged between 7 and 15 days, with very similar outcomes observed for both compounds,

Dose-response efficacy of X82107 and X82108

Upon demonstrating the promising effects of Ol conjugation on X82107 and X82108 variants, we further investigated the efficacy of these molecules at a higher dose (6mg/Kg), 15 days after the injection, when the effects of the 3 mg/Kg injection were already importantly reducedA single intravenous injection of 6 mg/kg of each variant was administered to HSA^{LR} mice (Fig. 6A,B, Supplemental dataset 1), and several parameters were evaluated . Specifically, both antimiRs led to significantly higher levels of MBNL protein in the skeletal muscles qd and gt compared to PBS-treated animals. However, the increase observed with X82108 was notably higher than with X82107 (Fig. 6C, Supplemental dataset 1). This trend was also reflected in the reduction of miR-23b levels, which decreased by up to 80% in X82108-treated animals (Supplemental dataset 1), and in a higher PSR achieved by this antimiR (Fig. 6D, Supplemental dataset 1). These molecular changes translated into functional improvements, with treated mice displaying similarly increased front leg grip strength, normalized to body weight (Fig. 6E, Supplemental dataset 1). Both candidates demonstrated a significant increase in PSR and normalized strength 15 days after injection at 6 mg/kg (Fig. 6F), confirming prolonged activity compared to results at the lower dose of 3 mg/kg conjugated with oleic acid or cholesterol *(52)*.

Docusign Envelope ID: 7E4C2DFC-1112-4D5D-8C31-F4048EAE7E40

Overall, both molecules exhibited a dose-dependent duration of effect, further supporting their potential as promising therapeutic candidates.

In vitro assessment of renal and immune activation profiles of X82107 and X82108

Potencial renal toxicity was assessed using an *in vitro* model with RPTEC/TERT1 cells, human renal proximal tubular epithelial cells modified with telomerase reverse transcriptase for long-term studies. RPTEC/TERT1 cells are ideal for nephrotoxicity, renal metabolism, and drug absorption studies, as they retain primary renal cell functions, including electrolyte transport, toxin response, and epithelial barrier integrity *(62)* and EGFR activation is a pivotal mediator for renal fibrosis and has a major role in activating pathways that mediate podocyte injury and loss in diabetic nephropathy *(63)* After treatment with antimiRs, extracellular epidermal growth factor (EGF) levels significantly increased at the highest dose of 100 µM for antimiR X82108 compared to PBS-treated controls (Fig. 7A), while a moderate but non-significant increase was observed for X82107 at the same dose (Fig. 7B). No substantial changes in EGF levels were detected at 1, 10, or 30 µM for either compound. Parallel MTS assays revealed significant cytotoxicity at 100 µM for both compounds, with cell viability inhibition exceeding 80% (Fig. 7C,D). This aligns with the accumulation of extracellular EGF, as non-viable cells have reduced EGF uptake capacity. In summary, significant effects on extracellular EGF levels and cell viability were observed only at 100 µM, a concentration typically associated with toxicity in these assays. At lower doses, both antimiRs displayed a favorable safety profile.

We also conducted *in vitro* tests in human blood to assess the potential immunogenic modulation and safety of lead candidates X82107 and X82108. Neither compound activated the complement

Docusign Envelope ID: 7E4C2DFC-1112-4D5D-8C31-F4048EAE7E40

system, as no increase in C3a was detected in serum or plasma samples, even at a high dose of 300 µM (Fig. 7E). Given that different chemical modifications in oligonucleotide-based drugs can significantly alter the pharmacokinetic and toxicological profiles of antisense ON, including potential effects on coagulation parameters *(64)*, we measured these parameters in normal human plasma. In coagulation assays, both X82107 and X82108 produced significantly prolonged activated partial thromboplastin time (aPTT, intrinsic coagulation pathway) at 30 µM and higher doses in normal human plasma, while prothrombin time (PT, extrinsic pathway) remained unchanged for both molecules compared to the PBS control (Fig. 7F). Platelet count and activation levels remained similar to control across all doses for both compounds (Fig. 7G). An additional assessment of cytokine release in human peripheral blood mononuclear cells (PBMCs) showed no significant cytokine increase following X82108 treatment (Fig. 7H). Overall, our preclinical data support a favorable toxicological profile for lead compounds X82107 and X82108, with no significant safety-related red flags.

AntimiR-23b-mediated upregulation of MBNL is a mechanism conserved in different mammal species

Human, rat (*Rattus norvegicus*) and pig (*Sus scrofa*) mature miR-23b sequences are identical. Considering this conservation, we tested the hypothesis that our lead antimiRs could similarly antagonize miR-23b function upon transfection and upregulate MBNL1 protein expression in cell lines from these species. Transfection of X82108 in fibroblasts of these two animals led to a significant increase of Mbnl1 levels and a dramatic reduction in the detection of miR-23b (Fig. 8A,B). Importantly, these results confirm that the inhibition of miR-23b produces Mbnl1 upregulation in different relevant preclinical mammalian species.

Docusign Envelope ID: 7E4C2DFC-1112-4D5D-8C31-F4048EAE7E40

To rule out cell line bias, X82107 and X82108 were tested on patient-derived primary myoblasts after 10 days of differentiation. This has already been reported for X82108 in *(35)* and is shown here for X82107 in two cell lines from that same study (Fig. 8C-E). Briefly, treatment of primary human myoblast cell lines MP09-57 (carrying 702 CTG repeats in *DMPK*) and MP10-31 (carrying 117 repeats) with X82107 resulted in a marked reduction of miR-23b detection (Fig. 8C). Overexpression of miR-23b and reduction in the presence of lead antimiRs correlated well with a significant increase of MBNL1 protein levels that approached or surpassed those observed in healthy control cells (MP-49F; Fig. 8D,E). Results from Fig. 8 and *(35)* demonstrate that lead antimiRs can significantly upregulate MBNL1 levels in diverse genetic backgrounds and CTG repeat expansion sizes.

DISCUSSION

We aimed to enhance the therapeutic potential of miR-23b inhibition in DM1 by developing optimized antimiRs. Inhibiting miR-23b has been shown to boost MBNL1 levels and counteract critical DM1 molecular defects. Given its elevated expression in DM1 *(35)*, we hypothesized that reducing miR-23b activity could mitigate disease effects. Starting with the non-optimized antimiR-23b molecule X820 (antagomiR-23b) *(52)*, we employed a two-step *in vitro* and *in vivo* screening strategy to refine miR-23b-targeting sequences, chemical modifications, and lipid conjugations, optimizing activity and toxicity in DM1 muscle cells. This approach combined the best features from each screening, yielding advanced candidates. Animal experiments confirmed the target engagement of these optimized molecules, validating the use of cell-based assays to streamline *in vivo* testing *(65)*.

Docusign Envelope ID: 7E4C2DFC-1112-4D5D-8C31-F4048EAE7E40

The PK/PD characteristics of ON drugs are strongly influenced by their chemical modifications and specific properties of the associated conjugates, if any *(59, 66)*. In DM1, any effective therapy must reach skeletal muscles, which can constitute up to approximately 40% of the total body mass in average healthy adults. However, the first clinical trial evaluating a therapeutic ON targeting *DMPK* transcripts in DM1 was discontinued due to insufficient drug levels in muscle tissue, even at the highest doses tested *(44)*. This underscores the inherent delivery challenges faced in treating genetic myopathies. Most ONs approved for human use are administered systemically by intravenous or s.c. injections to achieve broad distribution throughout the body. ON plasma concentration peaks immediately after administration, followed by rapid distribution to major body tissues within hours, except for the central nervous system *(47)*.

Receptor-specific delivery has been addressed by conjugating *DMPK*-degrading ONs to monoclonal antibodies or Fab fragments recognizing the transferrin receptor, aimed to enhance muscle tissue uptake *(9)*. The mechanism by which Ol conjugation may confer desirable properties to an ON has not been formally addressed, but an intriguing hypothesis is that lipids can facilitate the fusion with or disruption of the endosomal membrane, allowing the antisense ON to escape into the cytoplasm *(67, 68)*. ONs conjugated with fatty acids longer than C16 are known to form self-assembled vesicular structures, which may further enhance their intracellular delivery. The interaction of these fatty acid chains with mouse and human serum albumin (MSA/HSA) results in the formation of stable adducts, with a near-linear correlation between fatty acid-ON hydrophobicity and binding strength to albumin *(59, 60)*. This enhanced albumin binding likely prolongs circulation time, improves systemic stability, and facilitates efficient transport across endothelial barriers to reach target tissues, including skeletal muscle. These properties may

Docusign Envelope ID: 7E4C2DFC-1112-4D5D-8C31-F4048EAE7E40

collectively contribute to the superior therapeutic potential observed with Ol conjugated antimiRs. Importantly, while we compared unconjugated and conjugated ONs at the same dose in mg/kg, the higher molecular weight of the conjugated ONs means that fewer molecules were administered relative to their unconjugated counterparts. As a result, the observed increase in potency may be slightly underestimated, further underscoring the enhanced efficacy of the Ol-conjugated ONs.

The primary concern in early drug development for human use is safety, so we prioritized ON candidates that demonstrated the greatest therapeutic window. This prioritization strategy allowed for efficient progression from initial hits to lead candidates. Interestingly, significant toxicity was observed only at very high doses *in vitro* (e.g., 30-100 µM) of antimiRs for most of the compounds tested. This yielded remarkable differences of over 100-fold between the TC_{50} and the EC_{50} concentrations.

Our results indicate that lead compounds X82107 and X82108 do not activate human platelets or increase C3a in serum, with X82108 showing a slight, non-clinically meaningful prolongation in coagulation time at high doses. Overall, the compounds exhibit a safe toxicological profile, without adverse effects on coagulation or platelet activation.

Since miRNAs are short and highly conserved regulatory molecules, the same antimiR molecule can usually be tested in several mammalian animal models during regulatory preclinical steps *(69)*. In our case, after obtaining solid results in mice, we moved on to test our leading candidates in normal rat and pig fibroblasts. This was in anticipation of using minipigs as a large animal model in preclinical toxicology testing of antimiRs, given the numerous physiological similarities with humans, especially in cardiac studies *(70)*. Notably, these experiments confirmed that antimiR´s

Docusign Envelope ID: 7E4C2DFC-1112-4D5D-8C31-F4048EAE7E40

mechanism of action was conserved across mammalian species, even without expressing toxic CTG repeat expansions. Finally, the robust increase in MBNL1 levels in primary myoblast derived from two DM1 patients upon X82107 or X82108 *(35)* treatment demonstrated the effectiveness of these antimiRs across different human genetic backgrounds affected by DM1.

Studies with the original antagomiR-23b molecule determined an optimal dose of 12.5 mg/kg to significantly increase MBNL1 levels *in vivo (32)*. In comparison, the new lead candidates exhibited lower toxicity and higher potency, achieving the same effect on MBNL1 levels 5 days after administration with approximately four times lower dose (3 mg/kg) and sustaining this level of MBNL1 upregulation for at least 15 days with approximately half the dose (6 mg/kg). Notably, this enhanced potency also translated into improved alternative splicing correction, as reflected by a significantly higher overall PSR at both 3 mg/kg and 6 mg/kg doses, with the strongest splicing rescue observed at the peak of MBNL1 upregulation (Fig. 5B,C). While our study demonstrates the efficacy and safety of X82107 and X82108 in preclinical models, several limitations must be considered. First, although we observed robust MBNL1 upregulation and splicing correction, further studies are needed to evaluate whether these molecular improvements translate into sustained functional benefits beyond muscle strength and myotonia reduction. Additionally, while *in vivo* biodistribution analyses confirmed efficient skeletal muscle uptake, the extent of off-target effects in other tissues was not fully characterized by these experiments. Given the high conservation of miR-23b across species, the potential for unintended modulation of physiological pathways outside DM1-affected tissues were carefully examined in additional studies. Another key limitation is the absence of long-term toxicity data from these experiments, particularly

Docusign Envelope ID: 7E4C2DFC-1112-4D5D-8C31-F4048EAE7E40

regarding immune activation and hepatic or renal clearance after repeated dosing, which require further investigation in order to dose humans on a chronic basis.

To bridge the gap toward clinical application, the next steps were to include large-animal studies to confirm the efficacy and pharmacokinetics of these lead compounds in models with greater physiological similarity to humans, such as minipigs and non-human primates. Additionally, regulatory preclinical studies required detailed dose-escalation experiments to establish the maximum tolerated dose and long-term safety, particularly in the context of systemic administration. As ON-based therapies for neuromuscular diseases continue to evolve, complementary formulation strategies may further enhance the bioavailability and T_{index} of these compounds. Ultimately, clinical trial design will incorporate biomarker-driven endpoints, including MBNL1 target engagement and splicing correction, to facilitate a rigorous evaluation of therapeutic efficacy in DM1 patients.

Our approach, combining *in vitro* screening, rational design, and *in vivo* validation, efficiently identifies potent and safe candidates. This strategy enhances therapeutic development in the antimiR field and advances DM1 treatments by optimizing delivery and reducing toxicity.

MATERIALS AND METHODS

Study design

The design encompasses the optimization of antimiR-23b molecules and their testing both *in vitro* and *in vivo* to assess the efficacy, toxicity, and immune activation potential to select a lead compound with the highest potential for subsequent promotion to human use. For *in vitro* studies, antimiR candidates were screened using various chemical modifications and conjugates. The

Docusign Envelope ID: 7E4C2DFC-1112-4D5D-8C31-F4048EAE7E40

screening evaluated their EC_{50}, TC_{50}, and T_{index} in TDMs. The *in vivo* experiments used the DMSXL and *HSA*^{LR} mouse models. AntimiR candidates were administered to *HSA*^{LR} mice in different doses (3, 6, 100 mg/kg), and at 25 mg/kg to DMSXL mice, followed by evaluations of relative muscle strength and myotonia. Molecularly, key readouts included quantification of miRNA and MBNL1 protein and transcript levels, and alternative exon inclusion levels in skeletal muscles. Toxicity and immune activation assays were also conducted using multiple doses of the antimiRs. RPTEC-TERT1 cells were used to assess potential toxicities and cell proliferation, while human peripheral blood mononuclear cells (PBMCs) were utilized to measure cytokine release and complement activation.

Oligonucleotide synthesis

ON were provided by AXOLABS and resuspended in 1x PBS to prepare 5 mM stock solutions, stored at -20°C. 3´-oleyl-antimiRs were synthesized according to *(71)*. Supplementary Tables 1-3 include all the ON tested with sequence, modifications, length, tested concentrations, and TC_{50}, EC_{50}, E_{max} and T_{index} parameters of each one.

Cell culture experimentation

Immortalized MyoD-inducible (doxycycline) DM1 and control fibroblasts were kindly provided by Dr. Furling (Institute of Myology, Paris) and were grown in Dulbecco's Modified Eagle's Medium (DMEM) with 4.5 g/l glucose, 1% penicillin/streptomycin, and 10% FBS (Sigma, Saint Louis, Missouri) *(72)*. Fibroblast trans-differentiation into myotubes was performed according to *(32)*. Trans-differentiation was induced at day 0, and test compounds were added to the cell medium at the different concentrations indicated 24 h later by lipofection with X-tremeGENE™ HP (Roche, Basel, Switzerland) and were replaced with fresh differentiation medium 4 h

Docusign Envelope ID: 7E4C2DFC-1112-4D5D-8C31-F4048EAE7E40

afterward. Cells were collected on day 4 in the differentiation medium and processed for protein extraction.

RPTEC/TERT1 cells (CHT-003-0002, EVERCYTE GmbH) were cultured in phenol red-free DMEM/F12 medium (Gibco™ 11039021) supplemented with 1% penicillin/streptomycin, 3.5 µg/ml L-ascorbic acid (A4544), 25 ng/ml prostaglandin E1 (P5515), 8.65 ng/ml sodium selenite (S5261), 25 ng/ml hydrocortisone (H0396), 10 ng/ml human EGF (E9644), 5 µg/ml human insulin (I9278), 5 pM 3,3´,5-triiodo-L-thyronine (T6397), all from Sigma-Aldrich, 100 µg/ml geneticin (InvivoGen, ant-gn-5), 5 µg/ml human transferrin (Merck-Millipore, 616424), and 1% fetal bovine serum (Gibco™ 10270106). Cells were maintained in 25 cm^2 flasks and passaged 1–2 times per week using a 1:2 to 1:3 subculturing ratio, following the manufacturer's guidelines.

For ON toxicity assessment, RPTEC/TERT1 cells were seeded into 96-well plates (Greiner Bio-One™, 655180) at 20,000 cells/well in the specified medium and grown to confluence. On day 0, cells were treated with antimiRs prepared in PBS at final concentrations of 1, 10, 30, and 100 µM in 50 µl volumes. A toxic ON, SGLT2-MOE-ON (66), served as a positive control at 20, 300, 400, and 500 µM in 50 µl volumes. Final ON solutions were added to 150 µl of complete medium, with PBS as a vehicle control. On day 6, the medium was collected, centrifuged at 10,000 rpm to remove sediment, and the supernatants were stored at -80°C for EGF evaluation.

Primary myoblasts were grown on 0.1% gelatin-coated flasks in a proliferation medium containing DMEM supplemented with 10% FBS, 22% M-199, PSF 1x, insulin 1.74 µM, L-glutamine 2 mM, FGF 1.39 nM and EGF 0.135 mM. When the cells reached 80-90% of confluence, the medium was substituted by differentiation media containing DMEM supplemented with 2% FBS, 22% M-

Docusign Envelope ID: 7E4C2DFC-1112-4D5D-8C31-F4048EAE7E40

199, PSF 1x, insulin 1.74 μM and L-glutamine 2 mM. At this point, cells were transfected with X82107 at 100 nM using Ribocellin (BioCellChallenge, #RC1000) as a transfection reagent following the manufacturer's instructions. Cell pellets were collected for DNA, RNA, and protein analyses five days after differentiation started when treatments were also transfected.

Rat embryo (*Rat2*, ATCC CRL-1764) and pig testis (ST, ATCC CRL-1746) fibroblasts were grown in a complete medium (the same as for human fibroblasts) and seeded at 10^5 cells/ml in Petri plates. These cells were treated with X82108 at 50 nM and transfected with the same procedure as DM1 and control fibroblasts.

RNA extraction, semi-quantitative RT-PCR and RT-qPCR

Total RNA from murine gt and qd muscle was isolated using the miRNeasy Mini Kit (Qiagen, Hilden, Germany) according to the manufacturer's instructions. One microgram of RNA was digested with DNase I and reverse-transcribed with SuperScript II (Invitrogen, Carlsbad, California) using random hexanucleotides. For subsequent PCR reactions, 20 ng of cDNA was used with GoTaq polymerase (Promega, Madison, Wisconsin). Specific primers were used to analyze the alternative splicing of *Atp2a1*, *Nfix*, *Mbnl1*, and *Clcn1* in mouse samples (both muscles). *Gapdh* levels established the endogenous reference using 0.2 ng of cDNA. PCR products were separated on a 2% agarose gel and quantified using ImageJ software (NIH, Bethesda, Maryland). Percentage splice recovery index (PSR) per alternative exon was defined as the value: %EI minus $\bar{X}$%DEI, divided by $\bar{X}$%DEI minus $\bar{X}$%HEI (EI: exon inclusion of each sample; DEI: disease exon inclusion; HEI: healthy exon inclusion). Overall PSR was the average of the above PSR for the four alternative splicing events quantified and from the two muscles analyzed. The primer sequences and exons analyzed are available in *(32)*.

Docusign Envelope ID: 7E4C2DFC-1112-4D5D-8C31-F4048EAE7E40

We used 1 ng of mouse tissue cDNA as a template for multiplex RT-qPCR using the QuantiFast Probe PCR Kit reagent. Commercial TaqMan probes (Qiagen, Hilden, Germany) were used for mouse (*Mbnl1* and *Mbnl2*; FAM-labeled probes) and reference (*Gapdh* MAX-labeled probe) genes. Results were normalized to *Gapdh* endogenous gene expression. The sequences of the probes and primers are included in Supplementary Table 4.

MiRNA expression in muscle tissues was quantified using specific miRCURY™-locked nucleic acid microRNA PCR primers (Qiagen, Hilden, Germany) according to the manufacturer's instructions. Relative gene expression was normalized to U1 (YP00203909) and U6 (YP00203907) snRNAs. Expression levels were measured using a QuantStudio 5 Real-Time PCR System (Applied Biosystems, Foster City, California). Expression relative to the endogenous gene and control group was calculated using the $2^{-\Delta\Delta Ct}$ method.

Animal experimentation and antimiR administration

Mouse handling and experimental procedures for HSA^{LR} and FVB animals followed the European law regarding laboratory animal care and experimentation (2003/65/C.E.) and were approved by Conselleria de Agricultura, Generalitat Valenciana. Homozygous transgenic HSA^{LR} (line 20 b) mice *(73)* were provided by Prof. C. Thornton (University of Rochester Medical Center, Rochester, NY, USA). Experimental groups were FVB as wild-type control, HSA^{LR} treated with PBS as negative control, and HSA^{LR} mice treated with each of the experimental antimiRs. The sample size was four mice per treatment group, twelve mice for PBS, and eighteen mice for the FVB group. All groups were injected i.v. (tail vein) with 1× PBS (vehicle) or the specific antimiR with a single dose of 3 or 6 mg/kg, except for the 100 mg/kg group, which received a single s.c. injection. Five, seven or fifteen days after injection, the mice were sacrificed, and the tissues of interest were

Docusign Envelope ID: 7E4C2DFC-1112-4D5D-8C31-F4048EAE7E40

frozen in liquid nitrogen for molecular assays. Also, DMSXL mice (>99% C57BL/6 background) provided by Prof. G Gourdon (Sorbonne University, Paris, France), carrying over 1500 CTG repeats within the *DMPK* transgene*(74, 75)*, were used to study the effects of antimiR treatment (authorization APAFIS#30275-2021030414389550). These mice were three weeks old at the start of the experiment and received s.c. injections of antimiR X821 at a dose of 25 mg/kg, administered twice per week for four weeks. Age-matched wild-type littermate mice served as controls. Following the treatment regimen, the gastrocnemius and tibialis muscles were collected, rapidly frozen in liquid nitrogen, and stored at -80°C for subsequent molecular analyses.

Electromyography studies

Electromyography was performed before the treatment and at the time of sacrifice under general anesthesia, as previously described *(30)*.

Forelimb grip strength test

Forelimb grip strength was measured using a Grip Strength Meter (BIO-GS3; Bioseb, Pinellas Park, Florida). Peak pull strength (g) was recorded on a digital strength transducer as the mouse released its grip. The transducer was reset to 0 g after each measurement, and three measurements were taken at 30 s intervals. Body weight was recorded simultaneously, and normalized grip strength was calculated by dividing the average strength by body weight. Experiments were conducted with coded animals to prevent bias.

ELISA determinations

Custom hybridization-based ELISA determinations of antimiR conjugate concentrations in gt and qd from treated HSA^{LR} mice were performed as described in *(76)* using the following PS probe: miR-23b (5'->3') [BIO] ATCACATT$_o$G$_o$C$_o$C$_o$A$_o$G$_o$GGATTACC [DIG] double-labeled with

Docusign Envelope ID: 7E4C2DFC-1112-4D5D-8C31-F4048EAE7E40

digoxigenin (DIG) and biotin (BIO). A control sample (*HSA*^{LR} treated with PBS) was used to subtract the background.

Extracellular EGF assay

To determine extracellular EGF, Human EGF ELISA Kits (Invitrogen™ KHG0062) were used, and EGF concentration was determined according to manufacturer's instructions. The experimental protocol was adapted from *(77)*.

In vitro toxicity assay

The French Blood Donors Organization (EFS, Etablissement Français du Sang) provided human serum from healthy volunteers. Complement activation, coagulation, and platelet activation were performed by SQY Therapeutics (France) in human blood samples. Test compounds were incubated with human serum, and complement activation was evaluated using commercial ELISA measurement of human C3a. The extrinsic and intrinsic coagulation pathways were evaluated in human plasma incubated with test compounds. The PT and the aPTT were measured on a semi-automated START max coagulometer (Stago). Flow cytometry assays evaluated human platelet activation by test compounds by detecting surface antigens (usually glycoproteins) expressed during platelet activation. Assays with PBMCs were performed by Axolabs GmbH (Germany).

Statistical analyses

TC_{50} values were calculated using non-linear least-squares regression. For molecular and functional parameters, one-way ANOVA was performed where applicable, preceded by the Shapiro-Wilk normality test. Normal samples were Brown-Forsythe corrected if required, while non-normal samples were analyzed using Kruskal-Wallis without Dunn correction. Differences

Docusign Envelope ID: 7E4C2DFC-1112-4D5D-8C31-F4048EAE7E40

relative to control samples were assessed with two-tailed Student's t-tests ($\alpha = 0.05$), applying Welch's correction as needed. Sample sizes (n) are indicated in each figure.

The values obtained for the *HSA*^{LR} mice are represented (Fig. 4C) as the recovery index (RI), and it measures how close the different parameter values obtained with treated *HSA*^{LR} mice are from those of FVB controls. This RI is obtained for the different parameters (MBNL1 protein, *Mbnl1/2* and miR-23b or -218 expression level, PSR, *Mbnl1* ex5 inclusion recovery, and functional recovery) of each mouse after treatment according to this formula: value % MT minus X% MNT, divided by X% MH minus X% MNT (where MT is the value of each mice treated (PBS or oligonucleotide), MNT is *HSA*^{LR} mice treated with PBS (PBS), and MH is healthy mice value (FVB)). These values range from 0 to 100, where 0 are untreated mice (H*SA*^{LR}-PBS) and 100 are healthy mice (FVB).

List of Supplementary Materials

Supplementary Material and Methods
Tables S1 to S4
Figures S1 to S3
Supplemental Dataset 1

Acknowledgments:

We thank Inmaculada Noguera for veterinary assistance in the University of Valencia SCSIE animal facility. MDA Monoclonal Antibody Resources provided antibody MB1a (4A8).

Funding:

Docusign Envelope ID: 7E4C2DFC-1112-4D5D-8C31-F4048EAE7E40

"la Caixa" Banking Foundation grant HR17-00268 (RA, AL-M, GG).
Generalitat Valenciana grant PROMETEO/2020/081 (RA).
Instituto de Salud Carlos III grant DTS19/0128 (RA).
Generalitat Valenciana predoctoral grant FDEGENT/2020/011 (IG-M)
Torres Quevedo post-doctoral fellowship PTQ2020-011110 (EC-H)
CDTI NEOTEC grant SNEO-20201136 (BL)
GVA-IVACE grant IMIDTA/2021/65) (BL)
Talent Promotion Program-Line 3 of GVA-AVI INNTA3/2023/16 (DP-L).
Instituto de Salud Carlos III grant PI21/00557 (NN-G and AL-M)

Author contributions:

Conceptualization: RA, EC-H, BL.

Methodology: IG-M, MAV, NM, MC-S, NB.

Validation: EC-H, AG-R, DP-L, NB.

Formal analysis: IG-M, EC-H, MC-S, AG-R, DP-L, AC-R, MCH.

Investigation: IG-M, EC-H, MC-S, AG-R, DP-L, AC-R, MCH, AH-L, AG-B, NM, MD.

Resources: RA, NN-G, AL-M, GG.

Data Curation: -

Visualization: IG-M, EC-H.

Funding acquisition: RA, BL, AL-M, GG.

Project administration: RA, BL, AL-C.

Supervision: RA, EC-H, GG, AL-M.

Writing – original draft: RA, AL-C.

Writing – review & editing: RA, IG-M, EC-H, AL-C.

Docusign Envelope ID: 7E4C2DFC-1112-4D5D-8C31-F4048EAE7E40

Competing interests:

Beatriz Llamusi and Ruben Artero are founders, and CSO and scientific advisor of Arthex Biotech, respectively. B.LL, E.C-H and R.A, are co-inventors in patents PCT/EP2017/073685 (Modulation of microRNAs against myotonic dystrophy type 1 and antagonists of microRNAs therefor) and EP22382493 (Oligonucleotides conjugated to oleic acid and uses thereof), and IG-M also in the last one, currently licensed to Arthex Biotech. The remaining authors declare no competing interests.

Data and materials availability:

All materials used in this study are available upon reasonable request. AntimiRs will require a material transfer agreement. All data are available in the main text or the supplementary materials.

References

1. T. Ashizawa, C. Gagnon, W. J. Groh, L. Gutmann, N. E. Johnson, G. Meola, R. Moxley, S. Pandya, M. T. Rogers, E. Simpson, N. Angeard, G. Bassez, K. N. Berggren, D. Bhakta, M. Bozzali, A. Broderick, J. L. B. Byrne, C. Campbell, E. Cup, J. W. Day, E. De Mattia, D. Duboc, T. Duong, K. Eichinger, A. B. Ekstrom, B. van Engelen, B. Esparis, B. Eymard, M. Ferschl, S. M. Gadalla, B. Gallais, T. Goodglick, C. Heatwole, J. Hilbert, V. Holland, M. Kierkegaard, W. J. Koopman, K. Lane, D. Maas, A. Mankodi, K. D. Mathews, D. G. Monckton, D. Moser, S. Nazarian, L. Nguyen, P. Nopoulos, R. Petty, J. Phetteplace, J. Puymirat, S. Raman, L. Richer, E. Roma, J. Sampson, V. Sansone, B. Schoser, L. Sterling, J. Statland, S. H. Subramony, C. Tian, C. Trujillo, G. Tomaselli, C. Turner, S. Venance, A. Verma, M. White, S. Winblad, Consensus-based care recommendations for adults with myotonic dystrophy type 1. *Neurol Clin Pract* **8**, 507–520 (2018).

2. J. D. Brook, M. E. McCurrach, H. G. Harley, A. J. Buckler, D. Church, H. Aburatani, K. Hunter, V. P. Stanton, J. P. Thirion, T. Hudson, Molecular basis of myotonic dystrophy: expansion of a trinucleotide (CTG) repeat at the 3' end of a transcript encoding a protein kinase family member. *Cell* **68**, 799–808 (1992).

3. D. Savić Pavićević, J. Miladinović, M. Brkušanin, S. Šviković, S. Djurica, G. Brajušković, S. Romac, Molecular genetics and genetic testing in myotonic dystrophy type 1. *Biomed Res Int* **2013**, 391821 (2013).

4. M. S. Mahadevan, R. S. Yadava, M. Mandal, Cardiac Pathology in Myotonic Dystrophy Type 1. *Int J Mol Sci* **22**, 11874 (2021).

5. J. E. Hilbert, R. J. Barohn, P. R. Clemens, E. A. Luebbe, W. B. Martens, M. P. McDermott, A. L. Parkhill, R. Tawil, C. A. Thornton, R. T. Moxley, National Registry Scientific Advisory Committee/Investigators, High

Docusign Envelope ID: 7E4C2DFC-1112-4D5D-8C31-F4048EAE7E40

frequency of gastrointestinal manifestations in myotonic dystrophy type 1 and type 2. *Neurology* **89**, 1348–1354 (2017).

6. J. A. M. Peterson, T. A. Cooper, Clinical and Molecular Insights into Gastrointestinal Dysfunction in Myotonic Dystrophy Types 1 & 2. *Int J Mol Sci* **23**, 14779 (2022).

7. K. Okkersen, M. Buskes, J. Groenewoud, R. P. C. Kessels, H. Knoop, B. van Engelen, J. Raaphorst, The cognitive profile of myotonic dystrophy type 1: A systematic review and meta-analysis. *Cortex* **95**, 143–155 (2017).

8. B. G. van der Velden, K. Okkersen, R. P. Kessels, J. Groenewoud, B. van Engelen, H. Knoop, J. Raaphorst, Affective symptoms and apathy in myotonic dystrophy type 1 a systematic review and meta-analysis. *J Affect Disord* **250**, 260–269 (2019).

9. M. Pascual-Gilabert, R. Artero, A. López-Castel, The myotonic dystrophy type 1 drug development pipeline: 2022 edition. *Drug Discov Today* **28**, 103489 (2023).

10. L. L. Ozimski, M. Sabater-Arcis, A. Bargiela, R. Artero, The hallmarks of myotonic dystrophy type 1 muscle dysfunction. *Biol Rev Camb Philos Soc* **96**, 716–730 (2021).

11. I. Holt, S. Mittal, D. Furling, G. S. Butler-Browne, J. D. Brook, G. E. Morris, Defective mRNA in myotonic dystrophy accumulates at the periphery of nuclear splicing speckles. *Genes Cells* **12**, 1035–48 (2007).

12. E. S. Goers, J. Purcell, R. B. Voelker, D. P. Gates, J. A. Berglund, MBNL1 binds GC motifs embedded in pyrimidines to regulate alternative splicing. *Nucleic Acids Res* **38**, 2467–84 (2010).

13. R. Batra, K. Charizanis, M. Manchanda, A. Mohan, M. Li, D. J. Finn, M. Goodwin, C. Zhang, K. Sobczak, C. A. Thornton, M. S. Swanson, Loss of MBNL leads to disruption of developmentally regulated alternative polyadenylation in RNA-mediated disease. *Mol Cell* **56**, 311–322 (2014).

14. X. Lin, J. W. Miller, A. Mankodi, R. N. Kanadia, Y. Yuan, R. T. Moxley, M. S. Swanson, C. A. Thornton, Failure of MBNL1-dependent post-natal splicing transitions in myotonic dystrophy. *Hum Mol Genet* **15**, 2087–97 (2006).

15. N. M. Kuyumcu-Martinez, G. S. Wang, T. A. Cooper, Increased steady-state levels of CUGBP1 in myotonic dystrophy 1 are due to PKC-mediated hyperphosphorylation. *Mol Cell* **28**, 68–78 (2007).

16. E. T. Wang, A. J. Ward, J. M. Cherone, J. Giudice, T. T. Wang, D. J. Treacy, N. J. Lambert, P. Freese, T. Saxena, T. A. Cooper, C. B. Burge, Antagonistic regulation of mRNA expression and splicing by CELF and MBNL proteins. *Genome Res* **25**, 858–871 (2015).

17. F. Freyermuth, F. Rau, Y. Kokunai, T. Linke, C. Sellier, M. Nakamori, Y. Kino, L. Arandel, A. Jollet, C. Thibault, M. Philipps, S. Vicaire, B. Jost, B. Udd, J. W. Day, D. Duboc, K. Wahbi, T. Matsumura, H. Fujimura, H. Mochizuki, F. Deryckere, T. Kimura, N. Nukina, S. Ishiura, V. Lacroix, A. Campan-Fournier, V. Navratil, E. Chautard, D. Auboeuf, M. Horie, K. Imoto, K. Y. Lee, M. S. Swanson, A. L. de Munain, S. Inada, H. Itoh, K. Nakazawa, T. Ashihara, E. Wang, T. Zimmer, D. Furling, M. P. Takahashi, N. Charlet-Berguerand, Splicing misregulation of SCN5A contributes to cardiac-conduction delay and heart arrhythmia in myotonic dystrophy. *Nat Commun* **7**, 11067 (2016).

18. T. M. Wheeler, J. D. Lueck, M. S. Swanson, R. T. Dirksen, C. A. Thornton, Correction of ClC-1 splicing eliminates chloride channelopathy and myotonia in mouse models of myotonic dystrophy. *J Clin Invest* **117**, 3952–7 (2007).

19. R. S. Savkur, A. V. Philips, T. A. Cooper, Aberrant regulation of insulin receptor alternative splicing is associated with insulin resistance in myotonic dystrophy. *Nat Genet* **29**, 40–7 (2001).

Docusign Envelope ID: 7E4C2DFC-1112-4D5D-8C31-F4048EAE7E40

20. L. A. Cisco, M. T. Sipple, K. M. Edwards, C. A. Thornton, J. D. Lueck, Verapamil mitigates chloride and calcium bi-channelopathy in a myotonic dystrophy mouse model. *J Clin Invest* **134**, e173576 (2024).

21. S. O. Braz, J. Acquaire, G. Gourdon, M. Gomes-Pereira, Of Mice and Men: Advances in the Understanding of Neuromuscular Aspects of Myotonic Dystrophy. *Front Neurol* **9**, 519 (2018).

22. J. D. Thomas, R. Oliveira, J. Sznajder Ł, M. S. Swanson, Myotonic Dystrophy and Developmental Regulation of RNA Processing. *Compr Physiol* **8**, 509–553 (2018).

23. L. M. André, R. T. P. van Cruchten, M. Willemse, D. G. Wansink, (CTG)n repeat-mediated dysregulation of MBNL1 and MBNL2 expression during myogenesis in DM1 occurs already at the myoblast stage. *PLoS One* **14**, e0217317 (2019).

24. A. Manta, D. W. Stouth, D. Xhuti, L. Chi, I. A. Rebalka, J. M. Kalmar, T. J. Hawke, V. Ljubicic, Chronic exercise mitigates disease mechanisms and improves muscle function in myotonic dystrophy type 1 mice. *J Physiol* **597**, 1361–1381 (2019).

25. C. M. Chamberlain, L. P. Ranum, Mouse model of muscleblind-like 1 overexpression: skeletal muscle effects and therapeutic promise. *Hum Mol Genet* **21**, 4645–54 (2012).

26. J. Choi, K. E. Personius, M. DiFranco, W. Dansithong, C. Yu, S. Srivastava, D. M. Dixon, D. B. Bhatt, L. Comai, J. L. Vergara, S. Reddy, Muscleblind-Like 1 and Muscleblind-Like 3 Depletion Synergistically Enhances Myotonia by Altering Clc-1 RNA Translation. *EBioMedicine* **2**, 1034–1047 (2015).

27. K.-Y. Lee, H.-C. Chang, C. Seah, L.-J. Lee, Deprivation of Muscleblind-Like Proteins Causes Deficits in Cortical Neuron Distribution and Morphological Changes in Dendritic Spines and Postsynaptic Densities. *Front Neuroanat* **13**, 75 (2019).

28. E. T. Wang, N. A. L. Cody, S. Jog, M. Biancolella, T. T. Wang, D. J. Treacy, S. Luo, G. P. Schroth, D. E. Housman, S. Reddy, E. Lécuyer, C. B. Burge, Transcriptome-wide regulation of pre-mRNA splicing and mRNA localization by muscleblind proteins. *Cell* **150**, 710–724 (2012).

29. C. Sellier, E. Cerro-Herreros, M. Blatter, F. Freyermuth, A. Gaucherot, F. Ruffenach, P. Sarkar, J. Puymirat, B. Udd, J. W. Day, G. Meola, G. Bassez, H. Fujimura, M. P. Takahashi, B. Schoser, D. Furling, R. Artero, F. H. T. Allain, B. Llamusi, N. Charlet-Berguerand, rbFOX1/MBNL1 competition for CCUG RNA repeats binding contributes to myotonic dystrophy type 1/type 2 differences. *Nat Commun* **9**, 2009 (2018).

30. R. N. Kanadia, J. Shin, Y. Yuan, S. G. Beattie, T. M. Wheeler, C. A. Thornton, M. S. Swanson, Reversal of RNA missplicing and myotonia after muscleblind overexpression in a mouse poly(CUG) model for myotonic dystrophy. *Proc Natl Acad Sci U S A* **103**, 11748–53 (2006).

31. J. T. Gladman, M. Mandal, V. Srinivasan, M. S. Mahadevan, Age of Onset of RNA Toxicity Influences Phenotypic Severity: Evidence from an Inducible Mouse Model of Myotonic Dystrophy (DM1). *PLOS ONE* **8**, e72907 (2013).

32. E. Cerro-Herreros, M. Sabater-Arcis, J. M. Fernandez-Costa, N. Moreno, M. Perez-Alonso, B. Llamusi, R. Artero, miR-23b and miR-218 silencing increase Muscleblind-like expression and alleviate myotonic dystrophy phenotypes in mammalian models. *Nat Commun* **9**, 2482 (2018).

33. A. Piasecka, M. W. Szcześniak, M. Sekrecki, A. Kajdasz, Ł. J. Sznajder, A. Baud, K. Sobczak, MBNL splicing factors regulate the microtranscriptome of skeletal muscles. *Nucleic Acids Res* **52**, 12055–12073 (2024).

34. E. Cerro-Herreros, I. González-Martínez, N. Moreno, J. Espinosa-Espinosa, J. M. Fernández-Costa, A. Colom-Rodrigo, S. J. Overby, D. Seoane-Miraz, J. Poyatos-García, J. J. Vilchez, A. López de Munain, M. A. Varela, M. J.

Docusign Envelope ID: 7E4C2DFC-1112-4D5D-8C31-F4048EAE7E40

Wood, M. Pérez-Alonso, B. Llamusí, R. Artero, Preclinical characterization of antagomiR-218 as a potential treatment for myotonic dystrophy. *Mol Ther Nucleic Acids* **26**, 174–191 (2021).

35. E. Cerro-Herreros, J. Núñez-Manchón, N. Naldaiz-Gastesi, M. Carrascosa-Sàez, A. García-Rey, D. P. Losilla, I. González-Martínez, J. Espinosa-Espinosa, K. Moreno, J. Poyatos-García, J. J. Vilchez, A. L. de Munain, M. Suelves, G. Nogales-Gadea, B. Llamusí, R. Artero, AntimiR treatment corrects myotonic dystrophy primary cell defects across several CTG repeat expansions with a dual mechanism of action. *Sci Adv* **10**, eadn6525 (2024).

36. W. van Roon-Mom, C. Ferguson, A. Aartsma-Rus, From Failure to Meet the Clinical Endpoint to U.S. Food and Drug Administration Approval: 15th Antisense Oligonucleotide Therapy Approved Qalsody (Tofersen) for Treatment of SOD1 Mutated Amyotrophic Lateral Sclerosis. *Nucleic Acid Ther* **33**, 234–237 (2023).

37. M. Egli, M. Manoharan, Chemistry, structure and function of approved oligonucleotide therapeutics. *Nucleic Acids Res* **51**, 2529–2573 (2023).

38. A. Khvorova, J. K. Watts, The chemical evolution of oligonucleotide therapies of clinical utility. *Nat Biotechnol* **35**, 238–248 (2017).

39. F. Eckstein, Phosphorothioates, essential components of therapeutic oligonucleotides. *Nucleic Acid Ther* **24**, 374–387 (2014).

40. T. De Serres-Bérard, S. Ait Benichou, D. Jauvin, M. Boutjdir, J. Puymirat, M. Chahine, Recent Progress and Challenges in the Development of Antisense Therapies for Myotonic Dystrophy Type 1. *Int J Mol Sci* **23** (2022), doi:10.3390/ijms232113359.

41. K. S. Frazier, Antisense oligonucleotide therapies: the promise and the challenges from a toxicologic pathologist's perspective. *Toxicol Pathol* **43**, 78–89 (2015).

42. P. H. Hagedorn, V. Yakimov, S. Ottosen, S. Kammler, N. F. Nielsen, A. M. Høg, M. Hedtjärn, M. Meldgaard, M. R. Møller, H. Orum, T. Koch, M. Lindow, Hepatotoxic potential of therapeutic oligonucleotides can be predicted from their sequence and modification pattern. *Nucleic Acid Ther* **23**, 302–10 (2013).

43. F. Alhamadani, K. Zhang, R. Parikh, H. Wu, T. P. Rasmussen, R. Bahal, X. B. Zhong, J. E. Manautou, Adverse Drug Reactions and Toxicity of the Food and Drug Administration-Approved Antisense Oligonucleotide Drugs. *Drug Metab Dispos* **50**, 879–887 (2022).

44. Ionis Pharmaceuticals, Industry Updates On Drug Development (2018 Myotonic Dystrophy Foundation annual conference). Available online: https://www.myotonic.org/digital-academy/ionis-pharmaceuticals-industry-updates-drug-development-2018-mdf-annual-conference [accessed on 1 December 2022]. .

45. S. M. Hammond, A. Aartsma-Rus, S. Alves, S. E. Borgos, R. A. M. Buijsen, R. W. J. Collin, G. Covello, M. A. Denti, L. R. Desviat, L. Echevarría, C. Foged, G. Gaina, A. Garanto, A. T. Goyenvalle, M. Guzowska, I. Holodnuka, D. R. Jones, S. Krause, T. Lehto, M. Montolio, W. Van Roon-Mom, V. Arechavala-Gomeza, Delivery of oligonucleotide-based therapeutics: challenges and opportunities. *EMBO Mol Med* **13**, e13243 (2021).

46. K. M. Brown, J. K. Nair, M. M. Janas, Y. I. Anglero-Rodriguez, L. T. H. Dang, H. Peng, C. S. Theile, E. Castellanos-Rizaldos, C. Brown, D. Foster, J. Kurz, J. Allen, R. Maganti, J. Li, S. Matsuda, M. Stricos, T. Chickering, M. Jung, K. Wassarman, J. Rollins, L. Woods, A. Kelin, D. C. Guenther, M. W. Mobley, J. Petrulis, R. McDougall, T. Racie, J. Bombardier, D. Cha, S. Agarwal, L. Johnson, Y. Jiang, S. Lentini, J. Gilbert, T. Nguyen, S. Chigas, S. LeBlanc, U. Poreci, A. Kasper, A. B. Rogers, S. Chong, W. Davis, J. E. Sutherland, A. Castoreno, S. Milstein, M. K. Schlegel, I. Zlatev, K. Charisse, M. Keating, M. Manoharan, K. Fitzgerald, J.-T. Wu, M. A. Maier, V. Jadhav, Expanding RNAi therapeutics to extrahepatic tissues with lipophilic conjugates. *Nat Biotechnol* **40**, 1500–1508 (2022).

Docusign Envelope ID: 7E4C2DFC-1112-4D5D-8C31-F4048EAE7E40

47. R. S. Geary, D. Norris, R. Yu, C. F. Bennett, Pharmacokinetics, biodistribution and cell uptake of antisense oligonucleotides. *Adv Drug Deliv Rev* **87**, 46–51 (2015).

48. B. Malecova, R. S. Burke, M. Cochran, M. D. Hood, R. Johns, P. R. Kovach, V. R. Doppalapudi, G. Erdogan, J. D. Arias, B. Darimont, C. D. Miller, H. Huang, A. Geall, H. S. Younis, A. A. Levin, Targeted tissue delivery of RNA therapeutics using antibody-oligonucleotide conjugates (AOCs). *Nucleic Acids Res* **51**, 5901–5910 (2023).

49. O. Nakagawa, X. Ming, L. Huang, R. L. Juliano, Targeted intracellular delivery of antisense oligonucleotides via conjugation with small-molecule ligands. *J Am Chem Soc* **132**, 8848–8849 (2010).

50. A. Aartsma-Rus, D. R. Corey, The 10th Oligonucleotide Therapy Approved: Golodirsen for Duchenne Muscular Dystrophy. *Nucleic Acid Ther* **30**, 67–70 (2020).

51. T. Luo, C. Huo, T. Zhou, S. Xie, Progress on RNA-based therapeutics for genetic diseases. *Zhejiang Da Xue Xue Bao Yi Xue Ban* **52**, 406–416 (2023).

52. E. Cerro-Herreros, I. González-Martínez, N. Moreno-Cervera, S. Overby, M. Pérez-Alonso, B. Llamusí, R. Artero, Therapeutic Potential of AntagomiR-23b for Treating Myotonic Dystrophy. *Molecular Therapy - Nucleic Acids* **21**, 837–849 (2020).

53. X. Fernández-Garibay, M. A. Ortega, E. Cerro-Herreros, J. Comelles, E. Martínez, R. Artero, J. M. Fernández-Costa, J. Ramón-Azcón, Bioengineeredin vitro3D model of myotonic dystrophy type 1 human skeletal muscle. *Biofabrication* **13** (2021), doi:10.1088/1758-5090/abf6ae.

54. P. Y. Muller, M. N. Milton, The determination and interpretation of the therapeutic index in drug development. *Nat Rev Drug Discov* **11**, 751–761 (2012).

55. N. Moreno, I. González-Martínez, R. Artero, E. Cerro-Herreros, Rapid Determination of MBNL1 Protein Levels by Quantitative Dot Blot for the Evaluation of Antisense Oligonucleotides in Myotonic Dystrophy Myoblasts. *Methods Mol Biol* **2434**, 207–215 (2022).

56. D. M. Dincã, L. Lallemant, A. González-Barriga, N. Cresto, S. O. Braz, G. Sicot, L.-E. Pillet, H. Polvèche, P. Magneron, A. Huguet-Lachon, H. Benyamine, C. N. Azotla-Vilchis, L. E. Agonizantes-Juárez, J. Tahraoui-Bories, C. Martinat, O. Hernández-Hernández, D. Auboeuf, N. Rouach, C. F. Bourgeois, G. Gourdon, M. Gomes-Pereira, Myotonic dystrophy RNA toxicity alters morphology, adhesion and migration of mouse and human astrocytes. *Nat Commun* **13**, 3841 (2022).

57. M. E. Østergaard, M. Jackson, A. Low, A. E. Chappell, R. G. Lee, R. Q. Peralta, J. Yu, G. A. Kinberger, A. Dan, R. Carty, M. Tanowitz, P. Anderson, T.-W. Kim, L. Fradkin, A. E. Mullick, S. Murray, F. Rigo, T. P. Prakash, C. F. Bennett, E. E. Swayze, H. J. Gaus, P. P. Seth, Conjugation of hydrophobic moieties enhances potency of antisense oligonucleotides in the muscle of rodents and non-human primates. *Nucleic Acids Research* **47**, 6045–6058 (2019).

58. P. Tran, T. Weldemichael, Z. Liu, H. Li, Delivery of Oligonucleotides: Efficiency with Lipid Conjugation and Clinical Outcome. *Pharmaceutics* **14**, 342 (2022).

59. T. P. Prakash, A. E. Mullick, R. G. Lee, J. Yu, S. T. Yeh, A. Low, A. E. Chappell, M. E. Østergaard, S. Murray, H. J. Gaus, E. E. Swayze, P. P. Seth, Fatty acid conjugation enhances potency of antisense oligonucleotides in muscle. *Nucleic Acids Res* **47**, 6029–6044 (2019).

60. E.-A. Kusznir, J.-C. Hau, M. Portmann, A.-G. Reinhart, F. Falivene, J. Bastien, J. Worm, A. Ross, M. Lauer, P. Ringler, F. Sladojevich, S. Huber, K. Bleicher, M. Keller, Propensities of Fatty Acid-Modified ASOs: Self-Assembly vs Albumin Binding. *Bioconjug Chem* **34**, 866–879 (2023).

Docusign Envelope ID: 7E4C2DFC-1112-4D5D-8C31-F4048EAE7E40

61. S. Henry, K. Stecker, D. Brooks, D. Monteith, B. Conklin, C. F. Bennett, Chemically modified oligonucleotides exhibit decreased immune stimulation in mice. *J Pharmacol Exp Ther* **292**, 468–479 (2000).

62. B. R. Simon-Friedt, M. J. Wilson, D. A. Blake, H. Yu, Y. Eriksson, J. K. Wickliffe, The RPTEC/TERT1 Cell Line as an Improved Tool for In Vitro Nephrotoxicity Assessments. *Biol Trace Elem Res* **166**, 66–71 (2015).

63. H. Izzedine, M. A. Perazella, Adverse kidney effects of epidermal growth factor receptor inhibitors. *Nephrology Dialysis Transplantation* **32**, 1089–1097 (2017).

64. M. Dirin, J. Winkler, Influence of diverse chemical modifications on the ADME characteristics and toxicology of antisense oligonucleotides. *Expert Opin Biol Ther* **13**, 875–88 (2013).

65. I. González-Martínez, E. Cerro-Herreros, N. Moreno, A. García-Rey, J. Espinosa-Espinosa, M. Carrascosa-Sàez, D. Piqueras-Losilla, A. Arzumanov, D. Seoane-Miraz, Y. Jad, R. Raz, M. J. Wood, M. A. Varela, B. Llamusí, R. Artero, Peptide-conjugated antimiRs improve myotonic dystrophy type 1 phenotypes by promoting endogenous MBNL1 expression. *Molecular Therapy - Nucleic Acids* **34**, 102024 (2023).

66. R. L. Juliano, The delivery of therapeutic oligonucleotides. *Nucleic Acids Res* **44**, 6518–48 (2016).

67. A. González-Barriga, B. Nillessen, J. Kranzen, I. D. G. van Kessel, H. J. E. Croes, B. Aguilera, P. C. de Visser, N. A. Datson, S. A. M. Mulders, J. C. T. van Deutekom, B. Wieringa, D. G. Wansink, Intracellular Distribution and Nuclear Activity of Antisense Oligonucleotides After Unassisted Uptake in Myoblasts and Differentiated Myotubes In Vitro. *Nucleic Acid Ther* **27**, 144–158 (2017).

68. J. P. Leonetti, N. Mechti, G. Degols, C. Gagnor, B. Lebleu, Intracellular distribution of microinjected antisense oligonucleotides. *Proc Natl Acad Sci U S A* **88**, 2702–6 (1991).

69. D. de Rie, I. Abugessaisa, T. Alam, E. Arner, P. Arner, H. Ashoor, G. Åström, M. Babina, N. Bertin, A. M. Burroughs, A. J. Carlisle, C. O. Daub, M. Detmar, R. Deviatiiarov, A. Fort, C. Gebhard, D. Goldowitz, S. Guhl, T. J. Ha, J. Harshbarger, A. Hasegawa, K. Hashimoto, M. Herlyn, P. Heutink, K. J. Hitchens, C. C. Hon, E. Huang, Y. Ishizu, C. Kai, T. Kasukawa, P. Klinken, T. Lassmann, C.-H. Lecellier, W. Lee, M. Lizio, V. Makeev, A. Mathelier, Y. A. Medvedeva, N. Mejhert, C. J. Mungall, S. Noma, M. Ohshima, M. Okada-Hatakeyama, H. Persson, P. Rizzu, F. Roudnicky, P. Sætrom, H. Sato, J. Severin, J. W. Shin, R. K. Swoboda, H. Tarui, H. Toyoda, K. Vitting-Seerup, L. Winteringham, Y. Yamaguchi, K. Yasuzawa, M. Yoneda, N. Yumoto, S. Zabierowski, P. G. Zhang, C. A. Wells, K. M. Summers, H. Kawaji, A. Sandelin, M. Rehli, FANTOM Consortium, Y. Hayashizaki, P. Carninci, A. R. R. Forrest, M. J. L. de Hoon, An integrated expression atlas of miRNAs and their promoters in human and mouse. *Nat Biotechnol* **35**, 872–878 (2017).

70. C. K. Huang, S. Kafert-Kasting, T. Thum, Preclinical and Clinical Development of Noncoding RNA Therapeutics for Cardiovascular Disease. *Circ Res* **126**, 663–678 (2020).

71. N. Navarro, S. Serantes, A. Aviñó, C. Fàbrega, R. Eritja, Synthesis and Evaluation of 3′-Oleyl–Oligonucleotide Conjugates as Potential Cellular Uptake Enhancers. *Synlett* **35**, 721–727 (2023).

72. L. Arandel, M. Polay Espinoza, M. Matloka, A. Bazinet, D. De Dea Diniz, N. Naouar, F. Rau, A. Jollet, F. Edom-Vovard, K. Mamchaoui, M. Tarnopolsky, J. Puymirat, C. Battail, A. Boland, J. F. Deleuze, V. Mouly, A. F. Klein, D. Furling, Immortalized human myotonic dystrophy muscle cell lines to assess therapeutic compounds. *Dis Model Mech* **10**, 487–497 (2017).

73. A. Mankodi, E. Logigian, L. Callahan, C. McClain, R. White, D. Henderson, M. Krym, C. A. Thornton, Myotonic dystrophy in transgenic mice expressing an expanded CUG repeat. *Science* **289**, 1769–73 (2000).

Docusign Envelope ID: 7E4C2DFC-1112-4D5D-8C31-F4048EAE7E40

74. H. Seznec, A. S. Lia-Baldini, C. Duros, C. Fouquet, C. Lacroix, H. Hofmann-Radvanyi, C. Junien, G. Gourdon, Transgenic mice carrying large human genomic sequences with expanded CTG repeat mimic closely the DM CTG repeat intergenerational and somatic instability. *Hum Mol Genet* **9**, 1185–94 (2000).

75. A. E. Gudde, A. González-Barriga, W. J. van den Broek, B. Wieringa, D. G. Wansink, A low absolute number of expanded transcripts is involved in myotonic dystrophy type 1 manifestation in muscle. *Hum Mol Genet* **25**, 1648–62 (2016).

76. U. Burki, V. Straub, Ultrasensitive Hybridization-Based ELISA Method for the Determination of Phosphorodiamidate Morpholino Oligonucleotides in Biological samples. *Methods Mol Biol* **1565**, 265–277 (2017).

77. A. Moisan, M. Gubler, J. D. Zhang, Y. Tessier, K. Dumong Erichsen, S. Sewing, R. Gérard, B. Avignon, S. Huber, F. Benmansour, X. Chen, R. Villaseñor, A. Braendli-Baiocco, M. Festag, A. Maunz, T. Singer, F. Schuler, A. B. Roth, Inhibition of EGF Uptake by Nephrotoxic Antisense Drugs In Vitro and Implications for Preclinical Safety Profiling. *Mol Ther Nucleic Acids* **6**, 89–105 (2017).

78. N. Moreno, I. González-Martínez, R. Artero, E. Cerro-Herreros, Rapid Determination of MBNL1 Protein Levels by Quantitative Dot Blot for the Evaluation of Antisense Oligonucleotides in Myotonic Dystrophy Myoblasts. *Methods Mol Biol* **2434**, 207–215 (2022).

79. I. González-Martínez, E. Cerro-Herreros, N. Moreno, A. García-Rey, J. Espinosa-Espinosa, M. Carrascosa-Sàez, D. Piqueras-Losilla, A. Arzumanov, D. Seoane-Miraz, Y. Jad, R. Raz, M. J. Wood, M. A. Varela, B. Llamusí, R. Artero, Peptide-conjugated antimiRs improve myotonic dystrophy type 1 phenotypes by promoting endogenous MBNL1 expression. *Molecular Therapy - Nucleic Acids* **34**, 102024 (2023).

80. E. Cerro-Herreros, I. González-Martínez, N. Moreno-Cervera, S. Overby, M. Pérez-Alonso, B. Llamusí, R. Artero, Therapeutic Potential of AntagomiR-23b for Treating Myotonic Dystrophy. *Molecular Therapy - Nucleic Acids* **21**, 837–849 (2020).

Docusign Envelope ID: 7E4C2DFC-1112-4D5D-8C31-F4048EAE7E40

Tables and figures

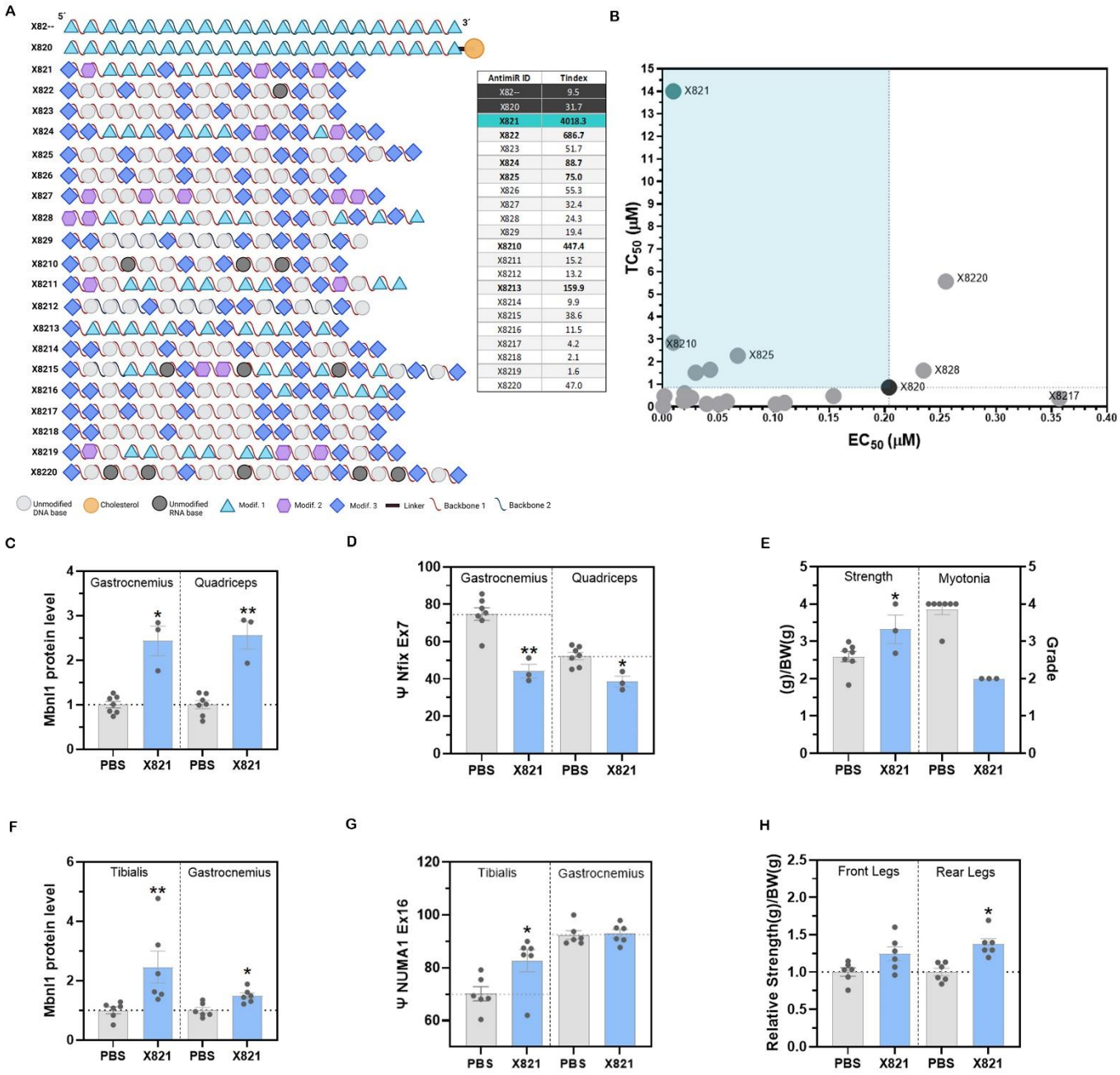

AntimiR ID	TIndex
X82--	9.5
X820	31.7
X821	**4018.3**
X822	**686.7**
X823	51.7
X824	**88.7**
X825	**75.0**
X826	55.3
X827	32.4
X828	24.3
X829	19.4
X8210	**447.4**
X8211	15.2
X8212	13.2
X8213	**159.9**
X8214	9.9
X8215	38.6
X8216	11.5
X8217	4.2
X8218	2.1
X8219	1.6
X8220	47.0

Docusign Envelope ID: 7E4C2DFC-1112-4D5D-8C31-F4048EAE7E40

Fig. 1. *In vitro* screening of antimiR-23b variants and assessment of safety and efficacy of a prospective lead in two mouse models. (A) Schematic representation of the antimiRs tested in the screening. Modifications 1, 2, and 3 refer to 2'-O-Methyl RNA nucleotides , 2'-O-MOE RNA nucleotides, and LNA nucleotides. Backbones 1 and 2 represent a mix of PS (phosphorothioate) and PO (phosphodiester) linkages.**(B)** Representative graphs illustrating the ranking of the compounds tested in the screening, based on their EC_{50} (µM) and TC_{50} (µM) values. The graph also includes a table displaying the T_{index} of each antimiR. In both the graph and the table, the benchmark compounds are indicated in dark gray, the antimiR hit of the screening in greenish-blue, and the remaining antimiRs in gray. The parameters measured in the two mouse models (*HSA*^{LR} (**C,D,E**) and DMSXL (**F,G,H**)) treated subcutaneously with X821 at SD 100 mg/kg and MD 25 mg/kg, respectively, were: **(C,F)** MBNL1 protein levels of treated mice relative to saline controls in skeletal muscles affected in DM1; **(D,G)** Quantification of the percentage of exon inclusion (Ψ) of the indicated exons and muscles. **(E,H)** Functional rescues after treatment: **(E)** relative force and myotonia grade change compared to controls; **(H)** change in relative muscle strength of antimiR-treated mice compared to saline controls at the indicated days after treatment. Error bars indicate mean ± SEM. *: $p<0.05$; **: $p<0.01$; ***: $p<0.001$. The data were analyzed using unpaired Student's t-tests, compared with untreated DM1 mice (PBS). AI: after injection; SD: single dose, MD: multiple dose. *HSA*^{LR}: PBS n=7, X821 n=3; DMSXL: PBS n=6, X821 n=6.

Docusign Envelope ID: 7E4C2DFC-1112-4D5D-8C31-F4048EAE7E40

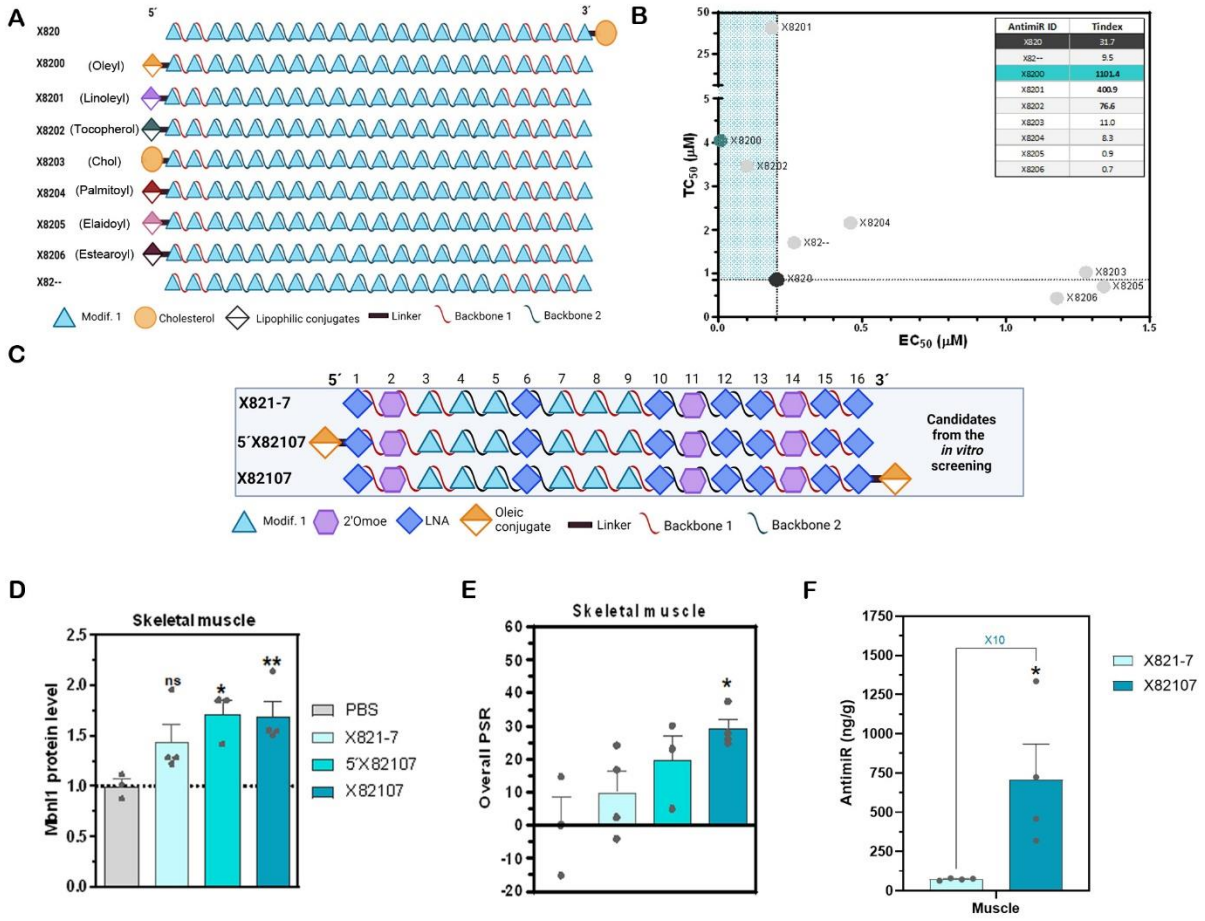

Fig. 2. *In vitro* screening of antimiRs-23b with different conjugates and assessment of safety and efficacy of a group of leads in *HSA^{LR}* mice. (**A**) Schematic representation of the antimiRs tested in the screening. Modifications 1, 2, and 3 refer to 2'-O-Methyl RNA nucleotides , 2'-O-MOE RNA nucleotides, and LNA nucleotides. Backbones 1 and 2 represent a mix of PS (phosphorothioate) and PO (phosphodiester) linkages. (**B**) Representative graph illustrating the ranking of the compounds tested based on their EC_{50} (µM) and TC_{50} (µM) values. The graph also includes a table displaying the T_{index} of each antimiR. In both the graph and the table, the benchmark compounds are indicated in dark gray, the antimiR hit of the screening in greenish-blue, and the remaining antimiRs in gray. **(C-F)** Selected compounds were tested *in vivo* using a i.v. 3 mg/kg single injection in *HSA^{LR}* mice. After five days, several parameters were measured, and skeletal muscle tissues were dissected for analysis. **(C)** Schematic representation of the antimiRs tested *in vivo* . **(D)** MBNL1 protein levels in skeletal muscle five days after injection

Docusign Envelope ID: 7E4C2DFC-1112-4D5D-8C31-F4048EAE7E40

(mean value of gt and qd). **(E)** Overall PSR score of leading antimiR candidates in both muscles. **(F)** AntimiR X82107 vs X821-7 levels in muscle tissues detected by ELISA. The multiplier value indicates the fold-change between the different versions tested. Error bars indicate mean ± SEM. *: $p<0.05$; ***: $p<0.001$. The data were analyzed by ANOVA one-way test or Kruskal-Wallis test when necessary, compared with untreated HSA^{LR} mice (PBS). Individual values are indicated as data points. PBS n=3, X821-7 n=4, 5'X82107 n=3, X82107 n=4.

Docusign Envelope ID: 7E4C2DFC-1112-4D5D-8C31-F4048EAE7E40

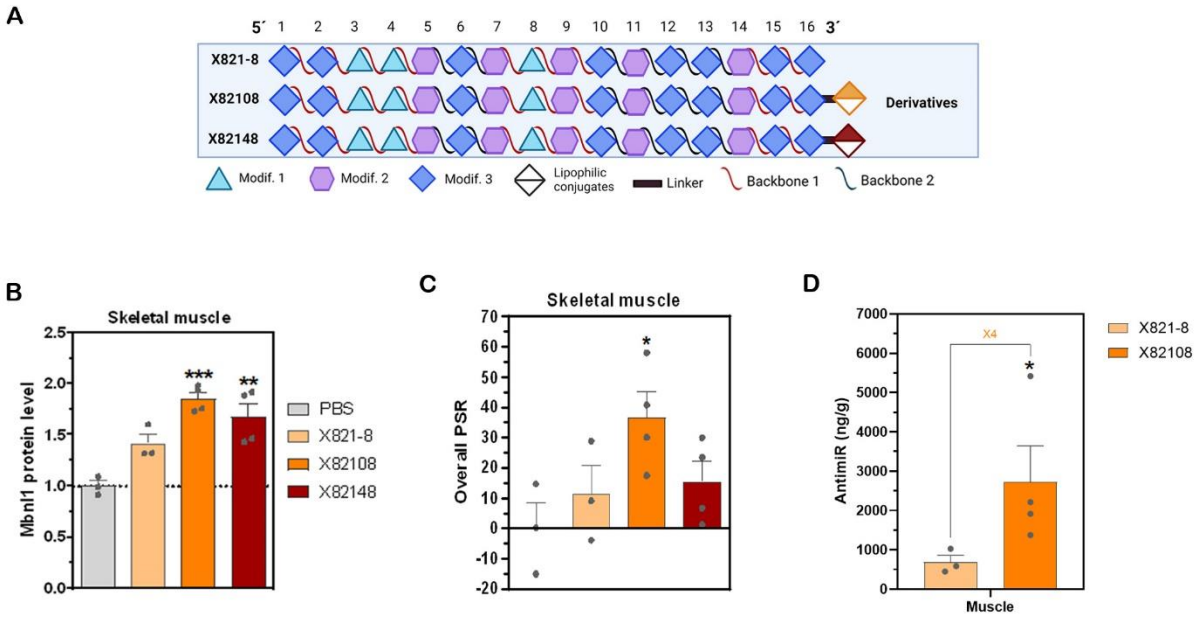

Fig. 3. Single-dose experiment with leading antimiR derivatives from the previous experiment. (A) Schematic representation of the antimiRs tested. Modifications 1, 2, and 3 refer to 2'-O-Methyl RNA nucleotides , 2'-O-MOE RNA nucleotides, and LNA nucleotides. Backbones 1 and 2 represent a mix of PS (phosphorothioate) and PO (phosphodiester) linkages. Selected compounds were tested *in vivo* using a i.v. 3 mg/kg single injection in HSA^{LR} mice. **(B)** MBNL1 protein levels in skeletal muscle (mean value of gt and qd). **(C)** Overall PSR score of leading antimiR candidates in both muscles. **(D)** AntimiR X82108 and X821-8 levels in muscle tissues (mean value of qd and gt) detected by ELISA. The multiplier value indicates the fold-change between the different versions tested. Error bars indicate mean ± SEM. *: $p<0.05$; **: $p<0.01$; ****: $p<0.0001$. The data were analyzed by ANOVA one-way test or Kruskal-Wallis test, when necessary, compared with untreated HSA^{LR} mice (PBS). Individual values are indicated as data points. PBS n=3, X821-8 n=3, X82108 n=4, X82148 n=4.

Docusign Envelope ID: 7E4C2DFC-1112-4D5D-8C31-F4048EAE7E40

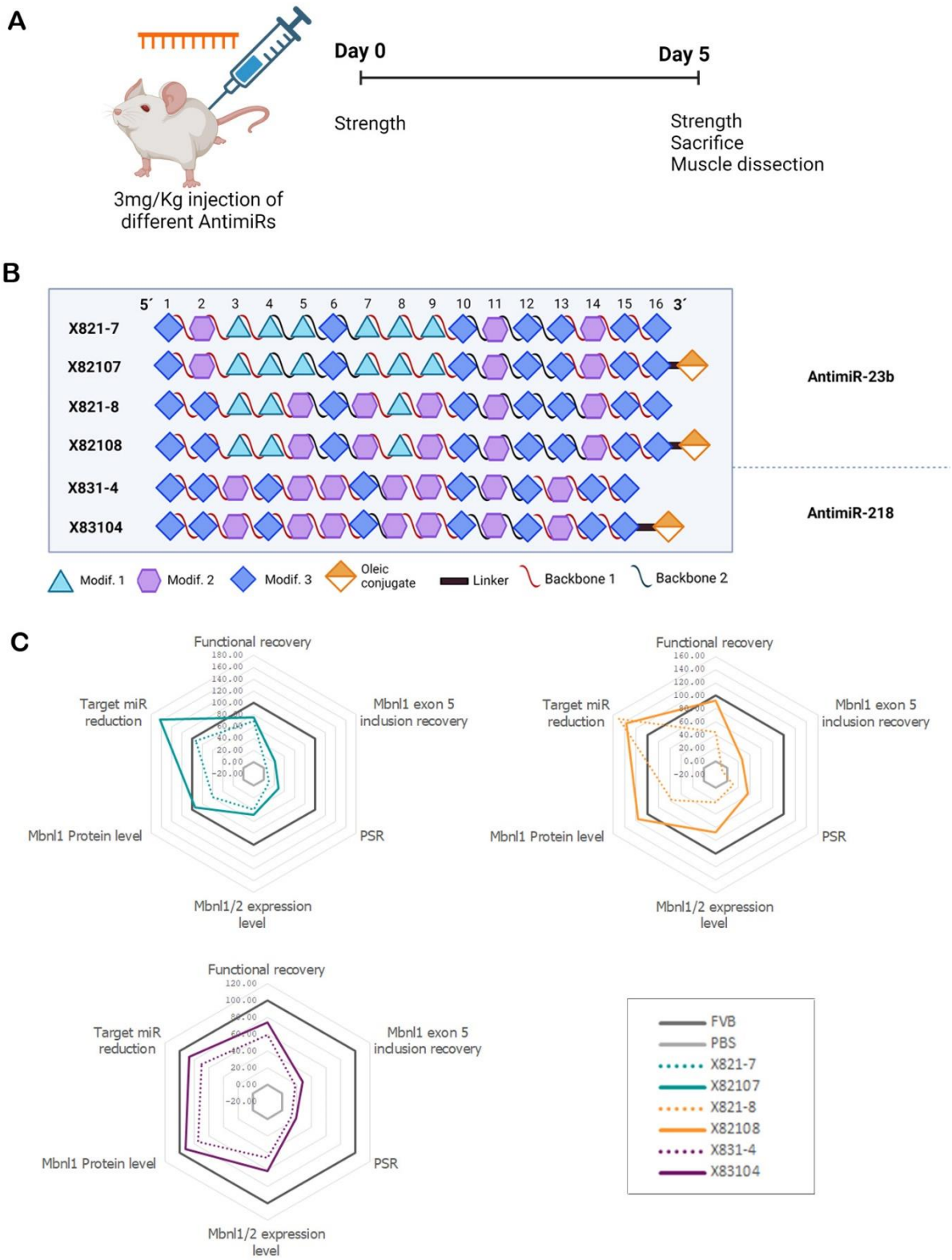

Docusign Envelope ID: 7E4C2DFC-1112-4D5D-8C31-F4048EAE7E40

Fig. 4. Effect of Oleyl conjugate in different antimiRs. (A) Scheme of the experimental design using a i.v. 3 mg/kg single injection in *HSA*^{LR} mice. Modifications 1, 2, and 3 refer to 2'-O-Methyl RNA nucleotides , 2'-O-MOE RNA nucleotides, and LNA nucleotides. Backbones 1 and 2 represent a mix of PS (phosphorothioate) and PO (phosphodiester) linkages. **(B)** Schematic representation of the antimiRs tested. **(C)** Spider graphs depicting the read-outs obtained in the *HSA*^{LR} mouse model with leading antimiR candidates. Functional recovery includes strength and myotonia measurements. PSR includes rescues of *Atp2a1* ex22, *Clcn1* ex7a, *Nfix* ex7 and *Mbnl1* ex5 in qd and gt. FVB n=5, PBS n=3, X821-7 n=4, X82107 n=3, X821-8 n=3, X82108 n=3, X831-4 n=4, X83104 n=4.

Docusign Envelope ID: 7E4C2DFC-1112-4D5D-8C31-F4048EAE7E40

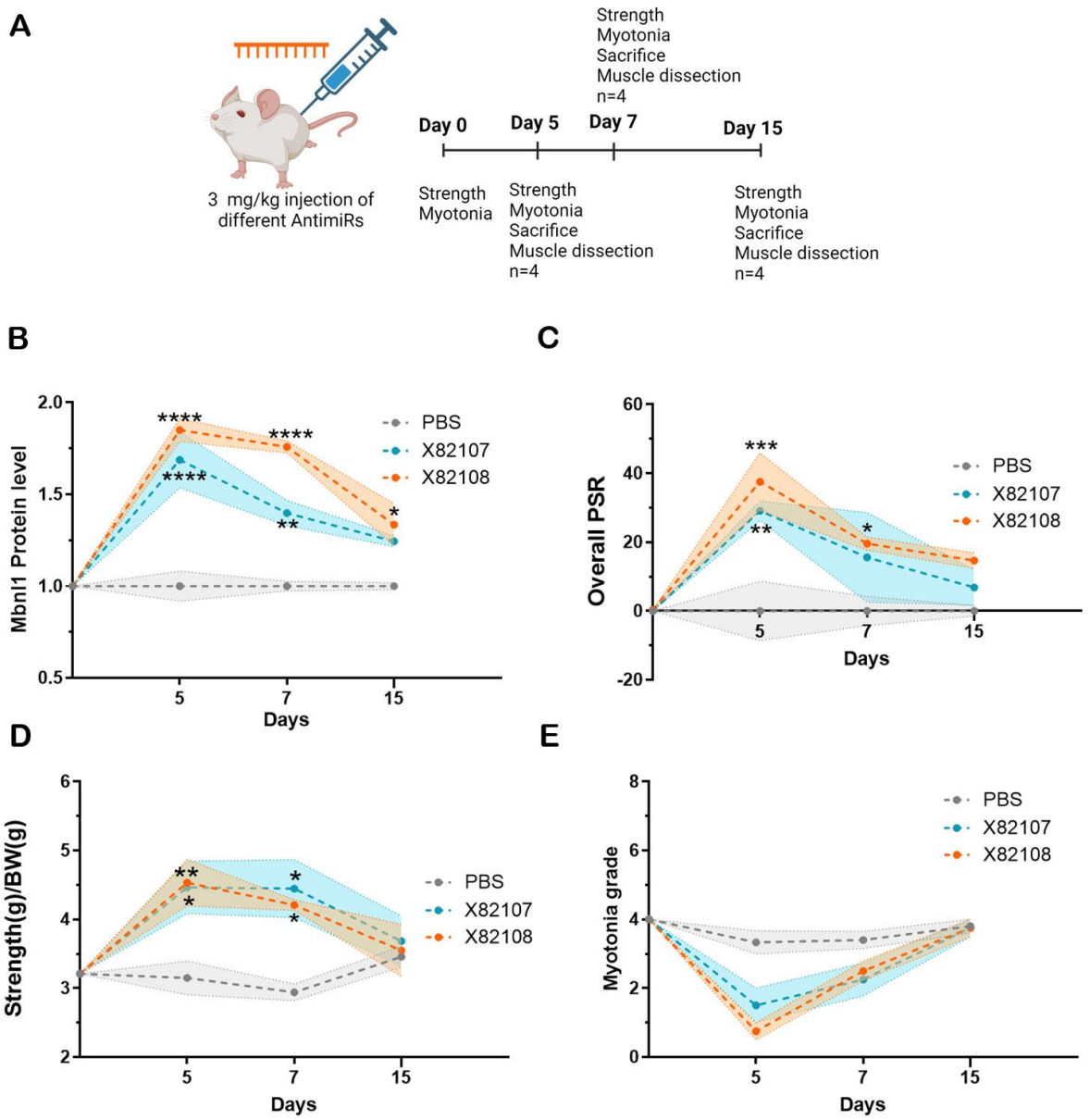

Figure 5. Selected antimiRs effects until 15 days. (A) Scheme of the experimental design using an i.v. 3 mg/kg single injection in *HSA*^{LR} mice. During fifteen days after the injection, several parameters were measured, and skeletal muscle tissues were collected for analysis: **(B)** MBNL1 protein levels and **(C)** overall PSR score in qd and gt muscles, **(D)** strength/body weight (g) and **(E)** myotonia grade at different time points after injection (AI). *: $p<0.05$; **: $p<0.01$; ***: $p<0.001$; ****: $p<0.0001$. The data were analyzed by ANOVA one-way test or Kruskal-Wallis test, when necessary, compared with untreated *HSA*^{LR} mice (PBS). The shaded area indicates the error in each case.

Docusign Envelope ID: 7E4C2DFC-1112-4D5D-8C31-F4048EAE7E40

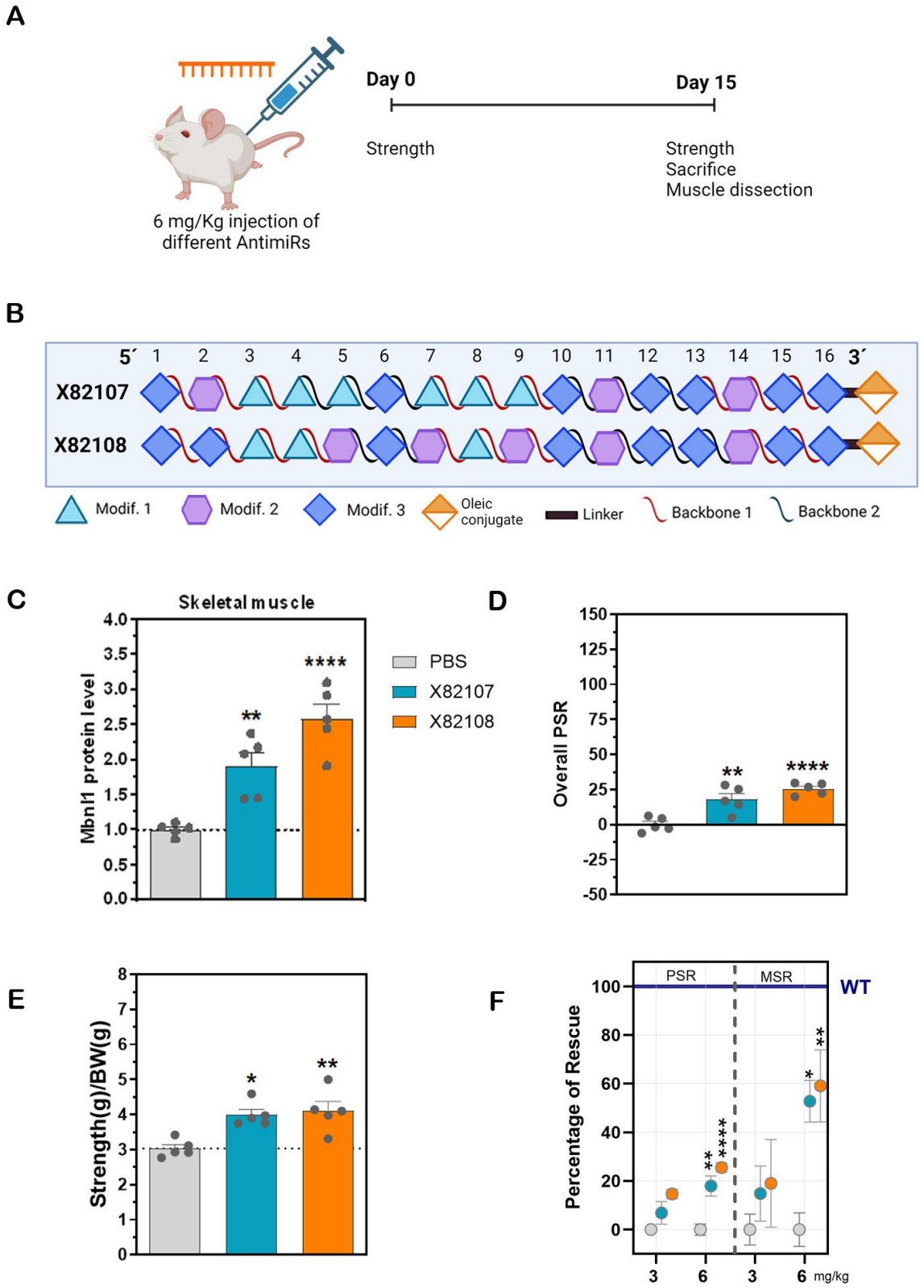

Docusign Envelope ID: 7E4C2DFC-1112-4D5D-8C31-F4048EAE7E40

Fig. 6. *In vivo* preclinical analysis with leading antimiR candidates. (A) Scheme of the experimental design using an i.v. 6 mg/kg single injection in *HSA*^{LR} mice. **(B)** Schematic representation of the antimiRs tested. Modifications 1, 2, and 3 refer to 2'-O-Methyl RNA nucleotides , 2'-O-MOE RNA nucleotides, and LNA nucleotides. Backbones 1 and 2 represent a mix of PS (phosphorothioate) and PO (phosphodiester) linkages. **(C)** MBNL1 protein levels in both muscles (mean value of qd and gt). **(D)** Overall PSR scores. **(E)** Front leg grip strength normalised to body weight. **(F)** Percentage of PSR and MSR (Muscle Strength Rescue) recues. Blue line indicates wild-type levels. Error bars indicate mean ± SEM. *: $p<0.05$; **: $p<0.01$; ***: $p<0.001$; ****: $p<0.0001$. The data were analyzed by ANOVA one-way test or Kruskal-Wallis test, when necessary, compared with untreated *HSA*^{LR} mice (PBS).

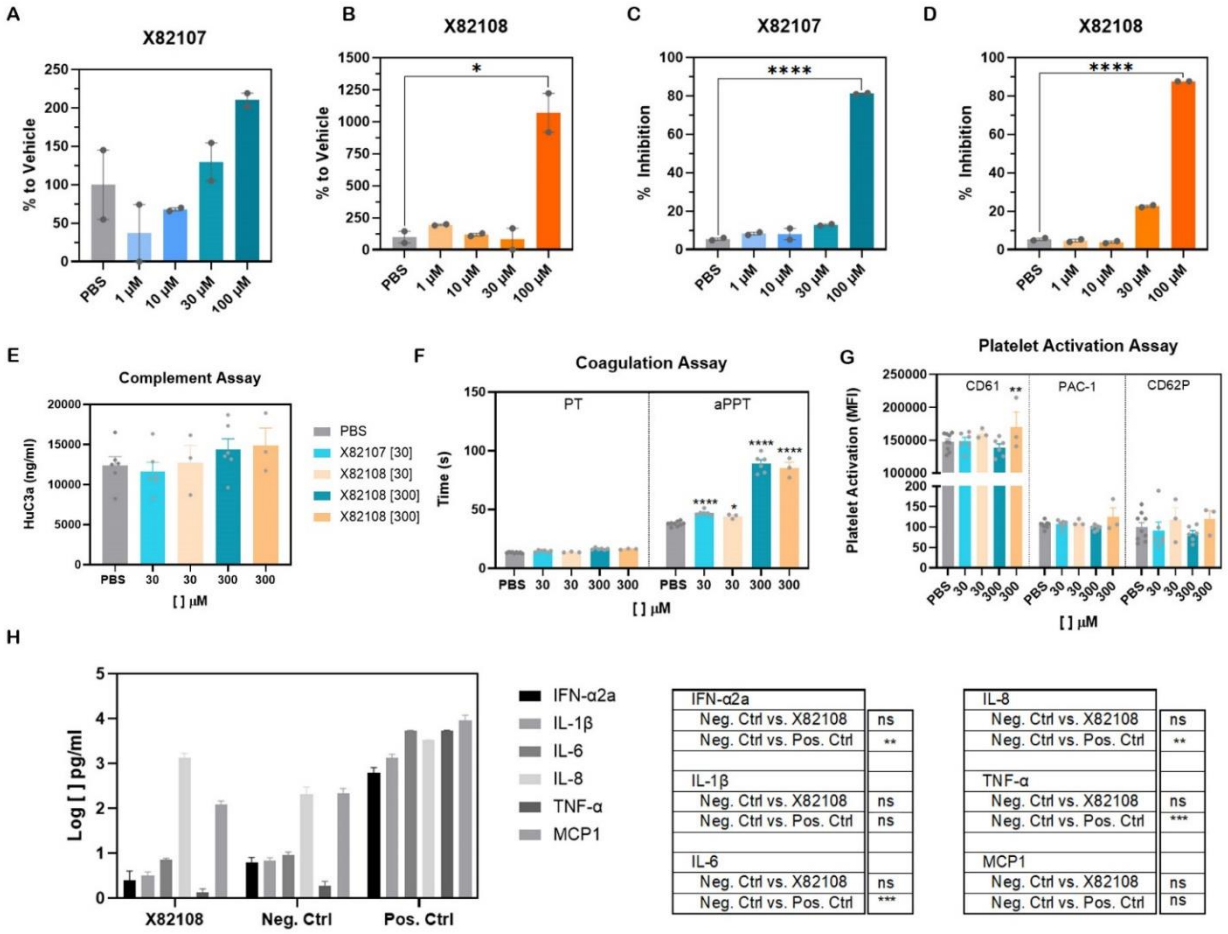

Docusign Envelope ID: 7E4C2DFC-1112-4D5D-8C31-F4048EAE7E40

Fig. 7. Toxicity and immune activation experiments with ascending doses of X82107 and X82108. EGF measurement **(A, B)** and Cell Proliferation Inhibition assay **(C, D)** in RPTEC/TERT1 cells upon antimiR treatment. **(E-H)** Immune activation analysis in blood samples from three different donors: **(E)** activated complement (C3a) measurement, **(F)** coagulation assay **(**prothrombin and activated partial thromboplastin times), **(G)** and total and activated platelet count as measured by several cell surface markers. **(H)** Cytokine release in human peripheral blood mononuclear cells (PBMCs) upon X82108 treatment. *: $p<0.05$; **: $p<0.01$; ***: $p<0.001$; ****: $p<0.0001$ according to ANOVA one-way test or Kruskal-Wallis test, when necessary, compared with negative control. aPPT: activated partial thromboplastin time; CD61: integrin beta-3; CD62P: platelet surface P-selectin; IFN: interferon; IL: interleukin; MCP1: monocyte chemoattractant protein-1; PAC1: activated GP IIb/IIIa; PBS: phosphate buffered saline; PT: prothrombin time; TNF: tumor necrosis factor.

Docusign Envelope ID: 7E4C2DFC-1112-4D5D-8C31-F4048EAE7E40

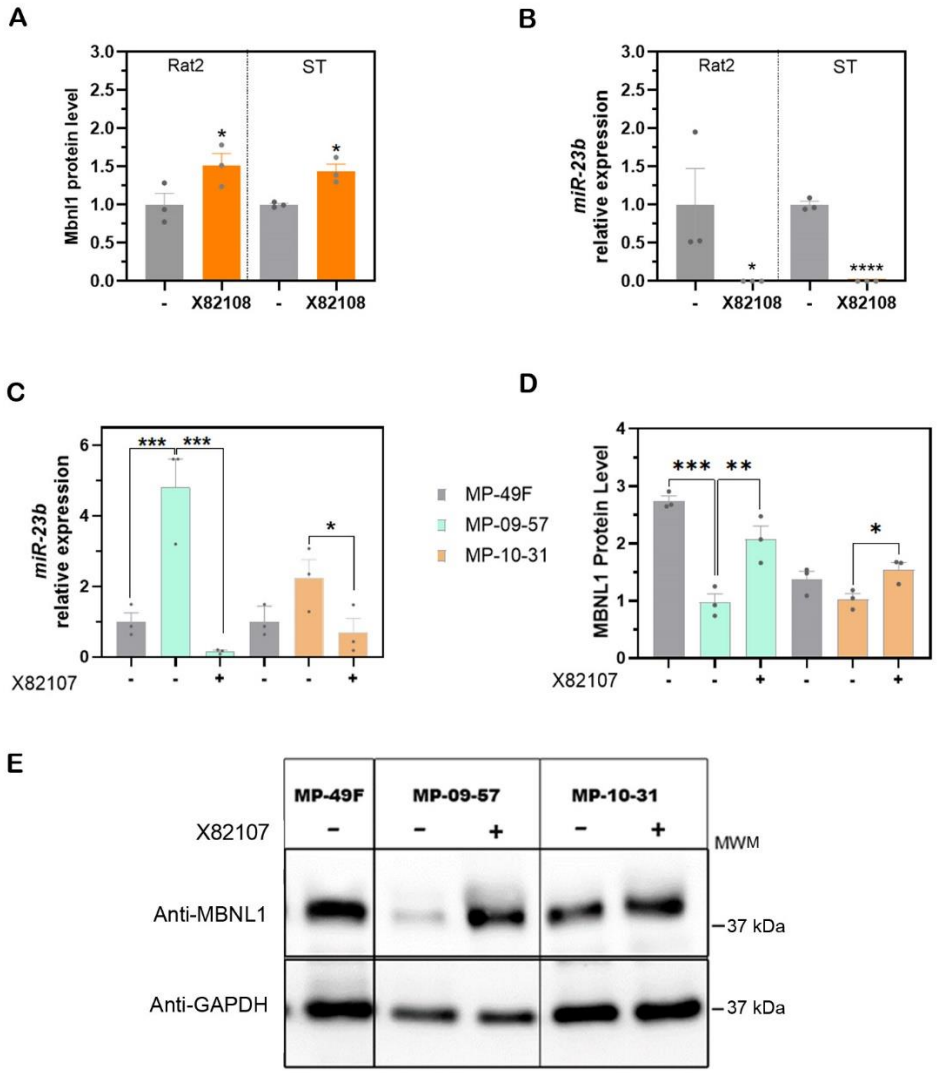

Fig. 8. Confirmation of the conservation of antimiR-23b regulation activity on MBNL levels in various cell types. (A) MBNL1 protein levels and **(B)** miR-23b relative levels in Rat2 and ST cells upon treatment with X82108. *: $p<0.05$, ****: $p<0.0001$ according to Student's t-test compared with non-treated cells; ST: *Sus scrofa* (testis). **(C)** miR-23b relative levels and **(D,E)** MBNL1 protein levels in primary myoblasts derived from DM1 patients upon treatment. MP-49F: control cell line; MP-09-57: DM1 cell line carrying 702 CTG repeats in *DMPK*; MP-10-31: DM1 cell line carrying 117 repeats. -: untreated; +: treated with X82107; *: p<0.05; **: p<0.01; ***: p<0.001. The data were analyzed by ANOVA one-way test or Kruskal-Wallis test when necessary, compared with untreated control cell line (MP-49F). ST: *Sus scrofa* (testis).

Docusign Envelope ID: 7E4C2DFC-1112-4D5D-8C31-F4048EAE7E40

Supp. Table 1. Screening of antimiR candidates: chemistry and sequences. The sequence for each oligonucleotide tested in DM1 TDMs are indicated. The dose range tested always included five levels, but lower concentrations were required for TC and EC determinations of certain compounds. The following parameters were calculated: EC_{50}, TC_{50}, E_{max} (maximum fold change), and T_{index} (therapeutic index). The grey rows show the results of a compound identical to the original antimiR-23b (20, 21) but from a provider that used a different linker between the oligonucleotide and the cholesterol moiety (X820), and an identical antimiR lacking the cholesterol, used as our benchmarks. Sequence key: N (A, G, T, C): DNA and RNA nucleotides and (C): 5-methyl-2'-O-methyl cytidine.

Name	Sequence (5' > 3')	TC_{50}	EC_{50}	E_{max}	T_{index}
X820	GGUAAUCCCUGGCAAUGUGAU-CHOLESTEROL	0,857	0,204	7,548	**31,7**
X82--	GGUAAUCCCUGGCAAUGUGAU	1,704	0,264	1,478	**9,5**
X821	AT(C)(C)(C)TGG(C)AATGTGA	14,000	0,010	2,870	**4018,3**
X822	C(C)(C)TGGCAATGUGAT	0,471	0,002	2,916	**686,7**
X823	C(C)(C)TGG(C)AATGTGAT	0,025	0,001	1,655	**51,7**
X824	AT(C)(C)(C)TGG(C)AATGTGAT	1,510	0,030	1,763	**88,7**
X825	TAATCCCTGGCAATGTGAT	2,271	0,068	2,247	**75,0**
X826	CCCTGGCAATGTGAT	0,598	0,019	1,758	**55,3**
X827	ATCCCTGGCAATGTGAT	0,263	0,019	2,343	**32,4**
X828	TAAT(C)(C)(C)TGGCAATGTGAT	1,604	0,235	3,564	**24,3**
X829	ATCCCTGGCAATGTGA	0,234	0,058	4,817	**19,4**
X8210	CCCUGGCAAUGUGAT	2,850	0,010	1,570	**447,4**
X8211	TAAT(C)C(C)TGG(C)AATGTGA	0,128	0,021	2,497	**15,2**
X8212	ATCCCTGGCAATGTGA	0,275	0,040	1,918	**13,2**
X8213	C(C)(C)UGGCAAUGUGAT	1,640	0,043	4,194	**159,9**
X8214	ATCCCTGGCAATGTGAT	0,117	0,026	2,191	**9,9**
X8215	GGUAAUC(C)(C)UGGCAAUGUGAT	0,400	0,051	4,924	**38,6**
X8216	AATCCCTGGCAATGTGAT	0,481	0,113	2,701	**11,5**
X8217	AATCCCTGGCAATGTGAT	0,370	0,357	4,078	**4,2**
X8218	ATCCCTGGCAATGTGAT	0,175	0,110	1,299	**2,1**
X8219	TAAT(C)C(C)TGG(C)AATGTGA	0,110	0,102	1,473	**1,6**
X8220	GGUAAUCCCUGGCAAUGUGAT	5,562	0,255	2,153	**47,0**

Docusign Envelope ID: 7E4C2DFC-1112-4D5D-8C31-F4048EAE7E40

Supp. Table 2. Screening of antimiR conjugate candidates. The sequence for each oligonucleotide used in DM1 TDMs is indicated. The following parameters were calculated: EC_{50}, TC_{50}, E_{max} (maximum fold change), and T_{index} (therapeutic index). The grey row shows the results for our benchmark antimiR-23b (35, 36). Sequence key: N (A, G, T, C): DNA and RNA nucleotides and (C): 5-methyl-2'-O-methyl cytidine.

Name	Sequence (5' > 3')	TC_{50}	EC_{50}	E_{max}	T_{index}
X820	GGUAAUCCCUGGCAAUGUGAU-CHOL	0,857	0,204	7,548	31,70
X82--	GGUAAUCCCUGGCAAUGUGAU	1,704	0,264	1,478	**9,53**
X8200	OLEYL-GGUAAUCCCUGGCAAUGUGAU	4,040	0,010	2,726	**1101,40**
X8201	LINOLEYL-GGUAAUCCCUGGCAAUGUGAU	40,630	0,186	1,835	**400,94**
X8202	TOCOPHEROL-GGUAAUCCCUGGCAAUGUGAU	3,460	0,100	2,211	**76,59**
X8203	CHOLESTEROL-GGUAAUCCCUGGCAAUGUGAU	1,027	1,279	13,654	**10,96**
X8204	PALMITOYL-GGUAAUCCCUGGCAAUGUGAU	2,156	0,460	1,775	**8,32**
X8205	ELAIDOYL-GGUAAUCCCUGGCAAUGUGAU	0,700	1,341	1,628	**0,85**
X8206	STEAROYL -GGUAAUCCCUGGCAAUGUGAU	0,432	0,730	1,848	**1,09**

Supp. Table 3. Leading antimiR candidates selected for further preclinical testing. Sequence key: N (A, G, T, C): DNA and RNA nucleotides and (C): 5-methyl-2'-O-methyl cytidine. The conjugate used in each case is indicated in the table.

Name	Sequence (5' > 3')
X821-7	AT(C)(C)(C)TGG(C)AATGTGA
5'X82107	OLEYL-AT(C)(C)(C)TGG(C)AATGTGA
X82107	AT(C)(C)(C)TGG(C)AATGTGA-OLEYL
X821-8	AT(C)(C)CTGGCAATGTGA
X82108	AT(C)(C)CTGGCAATGTGA-OLEYL
X82148	AT(C)(C)CTGGCAATGTGA-PALITOYL
X831-4	TTAGATCAAGCACAA
X83104	TTAGATCAAGCACAA-OLEYL

Docusign Envelope ID: 7E4C2DFC-1112-4D5D-8C31-F4048EAE7E40

Supp. Table 4. Probes and primers used for RT-qPCR. Sequence key: 6FAM: Fluorescein modification; IAbRQSp: Iowa Black RQ-Sp; MAX: NHS ester modification; BHQ_1: Black Hole Quencher-1.

Gene		Sequence (5'→3')
Mbnl1 (mouse)	**Probe**	/6FAM/TCGCAAATCAGCTGTGAGGAGATTCCCT/IAbRQSp/
	Primer Forward	TACCGATTGCACCACCAAAC
	Primer Reverse	GCTGCTTTCAGCAAAGTTGTC
Mbnl2 (mouse)	**Probe**	/6FAM/CCCGGCAGACAGCACCATGATCGA/IAbRQSp/
	Primer Forward	GAGACAGACTGCCGCTTTG
	Primer Reverse	GGTTACGGTGTTGTCGTTTGT
Gapdh	**Probe**	/MAX/-CGCCTGGTCACCAGGGCTGCT-/BHQ_1/
	Primer Forward	CAACGGATTTGGTCGTATTGG
	Primer Reverse	TGATGGCAACAATATCCACTTTACC

Docusign Envelope ID: 7E4C2DFC-1112-4D5D-8C31-F4048EAE7E40

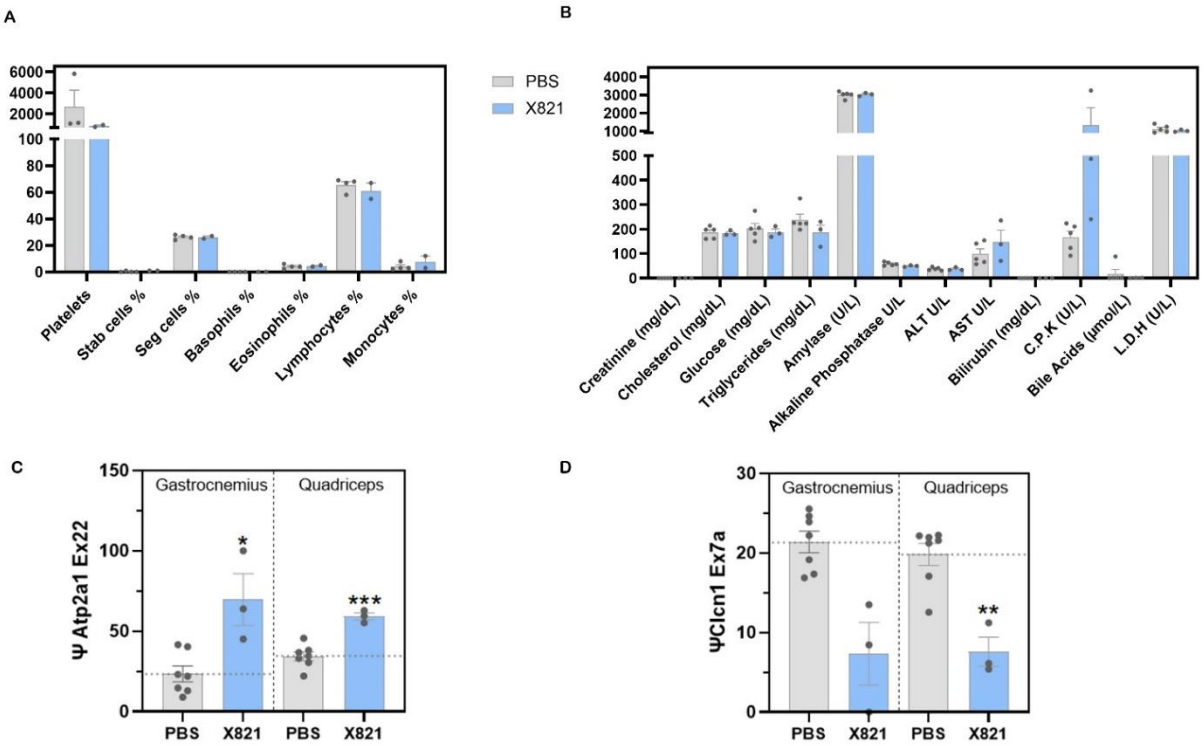

Fig. S1. Further safety and efficacy measurements of X821 treatment at 100 mg/kg in the *HSA^{LR}* mice. (A) White blood cell differential count and **(B)** blood serum biochemistry, measured in total blood extracted before sacrifice. **(C,D)** Quantification of the percentage of exon inclusion (Ψ) of the indicated exons and muscles. Error bars indicate mean ± SEM. *: p<0.05; **: p<0.01; ***: p<0.001. The data were analyzed by ANOVA one-way test or Kruskal-Wallis test when necessary, compared with untreated DM1 mice (PBS). PBS n=7, X821 n=3.

Docusign Envelope ID: 7E4C2DFC-1112-4D5D-8C31-F4048EAE7E40

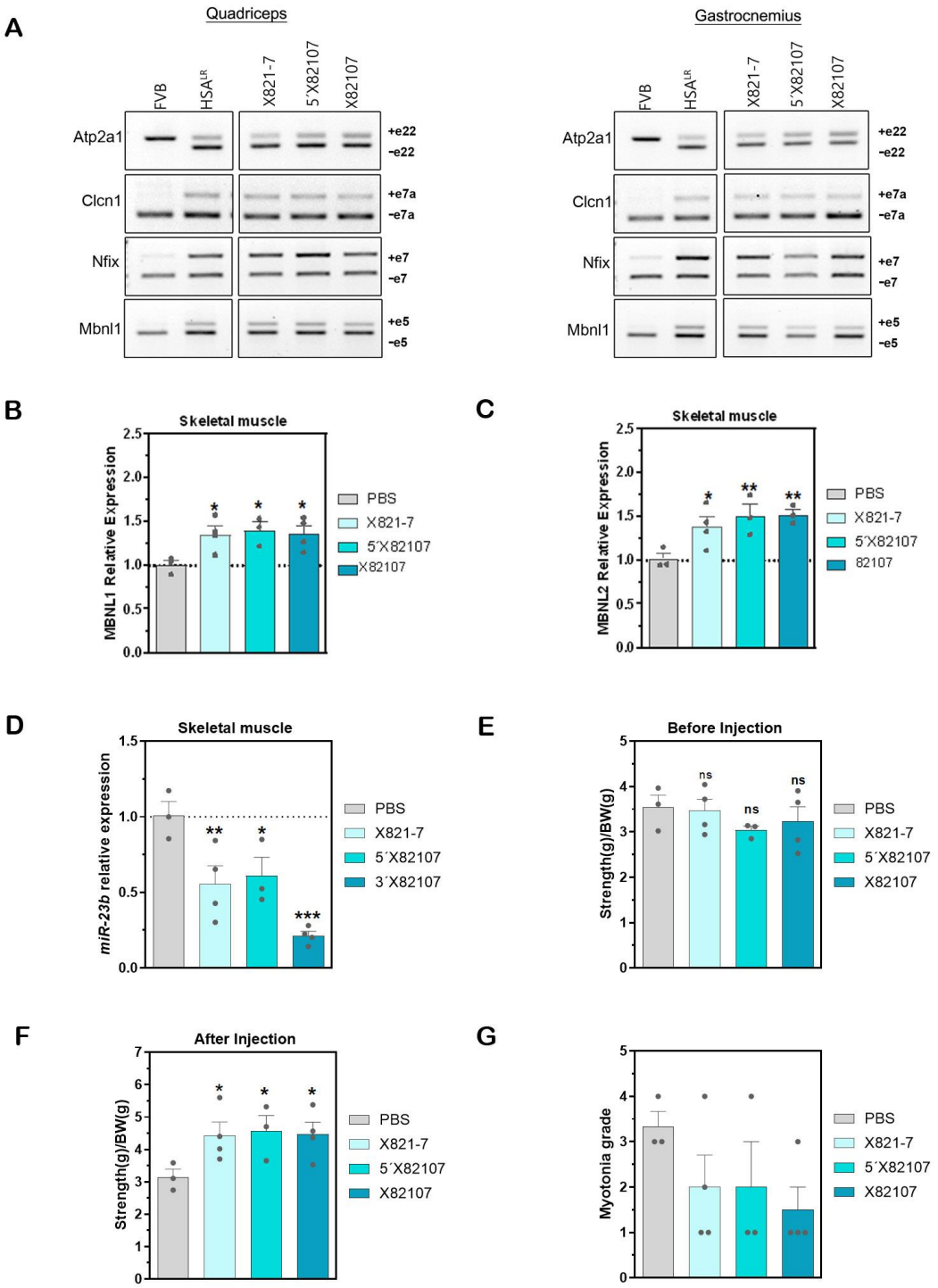

Fig. S2. Single-dose experiment with leading antimiR derivatives from the *in vitro* screening. Selected compounds were tested *in vivo* using a i.v. 3 mg/kg single injection in *HSA*^{LR} mice. After five days, several parameters were measured, and skeletal muscle tissues were dissected for analysis. Splice recovery of *Atp2a1* ex22, *Clcn1* ex7a, *Nfix* ex7, and *Mbnl1* ex5 in **(A)** quadriceps

Docusign Envelope ID: 7E4C2DFC-1112-4D5D-8C31-F4048EAE7E40

and gastrocnemius. **(B)** MBNL1, **(C)** MBNL2 and **(D)** miR-23b relative expression were also quantified after treatment. Functional recovery (E-F) strength and (G) myotonia) was measured **(E)** before and **(F-G)** after injection with the different tested compounds. Error bars indicate mean ± SEM. *: $p<0.05$; **: $p<0.01$; ***: $p<0.001$. The data were analyzed by ANOVA one-way test or Kruskal-Wallis test when it was necessary, compared with untreated HSA^{LR} mice (PBS). Individual values are indicated as data points. PBS n=3, X821-7 n=4, 5'X82107 n=3, X82107 n=4.

Docusign Envelope ID: 7E4C2DFC-1112-4D5D-8C31-F4048EAE7E40

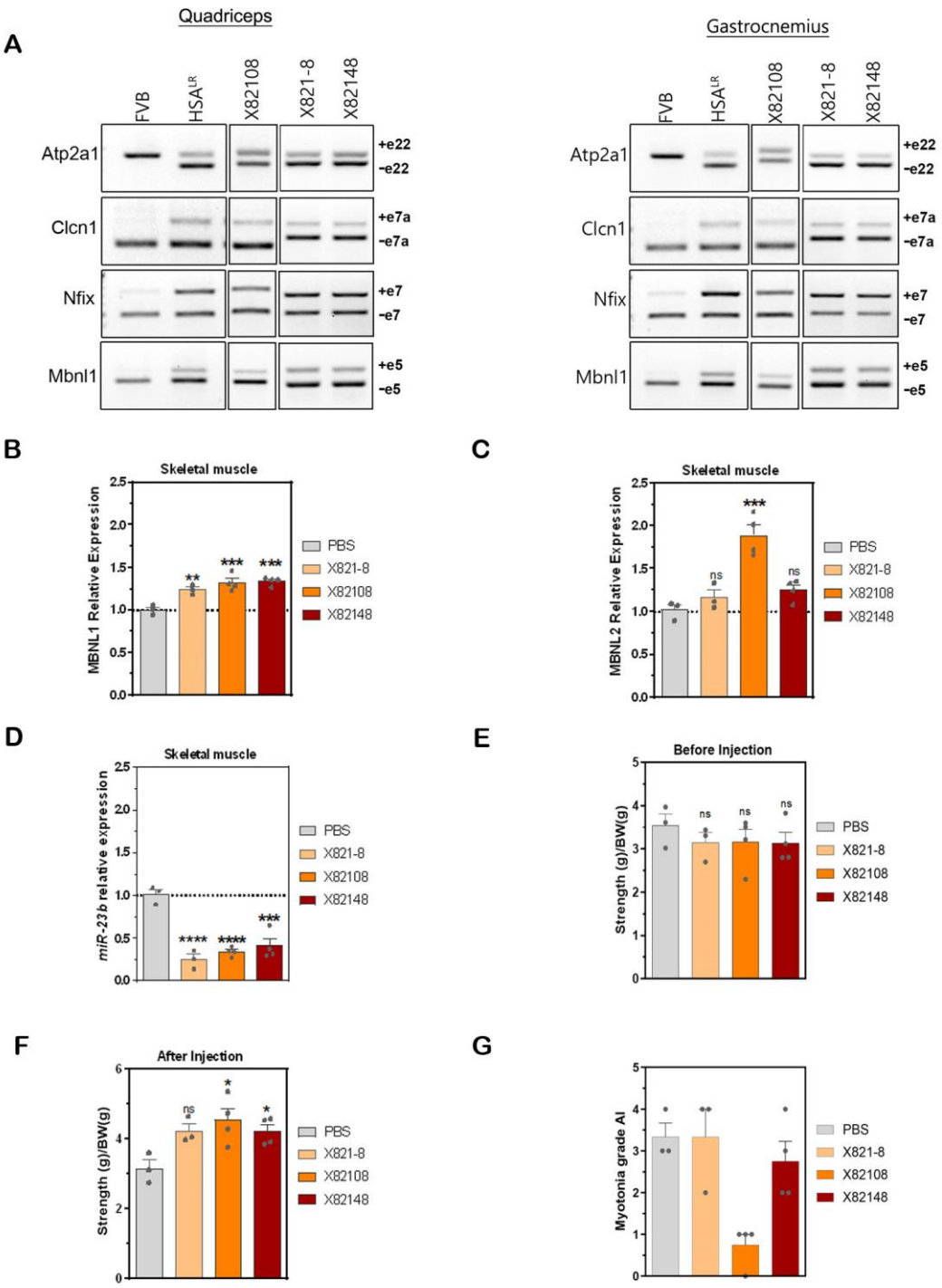

Fig. S3. Single-dose experiment with leading antimiR derivatives from the previous experiment. Selected compounds were tested *in vivo* using a i.v. 3 mg/kg single injection in HSA^{LR} mice. After five days, several parameters were measured, and skeletal muscle tissues were dissected for analysis. Splice recovery of *Atp2a1* ex22, *Clcn1* ex7a, *Nfix* ex7, and *Mbnl1* ex5 in

Docusign Envelope ID: 7E4C2DFC-1112-4D5D-8C31-F4048EAE7E40

(A) quadriceps and gastrocnemius. **(B)** MBNL1, **(C)** MBNL2 and **(D)** miR-23b relative expression were also quantified after treatment. Functional recovery (E-F) strength and (G) myotonia) was measured **(E)** before and **(F-G)** after injection with the different tested compounds. Error bars indicate mean ± SEM. *: $p<0.05$; **: $p<0.01$; ***: $p<0.001$; ****: $p<0.0001$. The data were analyzed by ANOVA one-way test or Kruskal-Wallis test when necessary, compared with untreated HSA^{LR} mice (PBS). Individual values are indicated as data points. PBS n=3, X821-8 n=3, X82108 n=4, X82148 n=4.

Docusign Envelope ID: 7E4C2DFC-1112-4D5D-8C31-F4048EAE7E40

SUPPLEMENTARY MATERIALS AND METHODS

Cell proliferation assay

DM1 and control fibroblasts seeded at 10^5 cells/ml in 96-well plates were transfected 24 h later with antimiRs, as previously described; after 96 h, cell proliferation was measured using the CellTiter 96® Aqueous Non-Radioactive Cell Proliferation Assay (Promega, Madison, Wisconsin). The absorbance levels were determined using an Infinite M200 PRO plate reader (Tecan, Männedorf, Switzerland). RPTEC/TERT1 cells were seeded into 96-well plates (Greiner Bio-One™, 655180), at a 20,000 cells/well density, and treated as previously explained. Cell viability was determined using the same procedure as fibroblasts upon medium harvesting on day six.

Protein extraction, Quantitative Dot Blot (QDB) and western blot (wb) assays

For the activity assay, cells were seeded in 6-well plates at a density of $8x10^4$ cells per well and transfected 24 h later with antimiRs, as described in the previous sections. For total protein extraction, human muscle cells were sonicated while mouse muscles (gastrocnemius, and quadriceps) were homogenized in Pierce® RIPA buffer (Thermo Scientific, Waltham, Massachusetts) supplemented with protease and phosphatase inhibitor cocktails (Roche Applied Science, Penzberg, Germany). Total protein was quantified with a Pierce® BCA protein assay kit (Thermo Scientific, Waltham, Massachusetts) using bovine serum albumin as standard. For the immunodetection assay, 1 µg/well of cell and 2 µg/well of mice samples were denatured (100°C for 5 min) and loaded in QDB plates (Quanticision Diagnostics Inc, Research Triangle Park, North Carolina). Quantifications by QDB were performed as described in *(78, 79)*. Quantifications of Mbnl1 protein levels by western blot were as described in *(80)*.

Docusign Envelope ID: 7E4C2DFC-1112-4D5D-8C31-F4048EAE7E40

SUPPLEMENTARY FIGURES AND TABLES

Supp. Table 1. Screening of antimiR candidates: chemistry and sequences. The sequence for each oligonucleotide tested in DM1 TDMs are indicated. The dose range tested always included five levels, but lower concentrations were required for TC and EC determinations of certain compounds. The following parameters were calculated: EC_{50}, TC_{50}, E_{max} (maximum fold change), and T_{index} (therapeutic index). The grey rows show the results of a compound identical to the original antimiR-23b (20, 21) but from a provider that used a different linker between the oligonucleotide and the cholesterol moiety (X820), and an identical antimiR lacking the cholesterol, used as our benchmarks. Sequence key: N (A, G, T, C): DNA and RNA nucleotides and (C): 5-methyl-2'-O-methyl cytidine.

Name	Sequence (5' > 3')	TC_{50}	EC_{50}	E_{max}	T_{index}
X820	GGUAAUCCCUGGCAAUGUGAU-CHOLESTEROL	0,857	0,204	7,548	**31,7**
X82--	GGUAAUCCCUGGCAAUGUGAU	1,704	0,264	1,478	**9,5**
X821	AT(C)(C)(C)TGG(C)AATGTGA	14,000	0,010	2,870	**4018,3**
X822	C(C)(C)TGGCAATGUGAT	0,471	0,002	2,916	**686,7**
X823	C(C)(C)TGG(C)AATGTGAT	0,025	0,001	1,655	**51,7**
X824	AT(C)(C)(C)TGG(C)AATGTGAT	1,510	0,030	1,763	**88,7**
X825	TAATCCCTGGCAATGTGAT	2,271	0,068	2,247	**75,0**
X826	CCCTGGCAATGTGAT	0,598	0,019	1,758	**55,3**
X827	ATCCCTGGCAATGTGAT	0,263	0,019	2,343	**32,4**
X828	TAAT(C)(C)(C)TGGCAATGTGAT	1,604	0,235	3,564	**24,3**
X829	ATCCCTGGCAATGTGA	0,234	0,058	4,817	**19,4**
X8210	CCCUGGCAAUGUGAT	2,850	0,010	1,570	**447,4**
X8211	TAAT(C)C(C)TGG(C)AATGTGA	0,128	0,021	2,497	**15,2**
X8212	ATCCCTGGCAATGTGA	0,275	0,040	1,918	**13,2**
X8213	C(C)(C)UGGCAAUGUGAT	1,640	0,043	4,194	**159,9**
X8214	ATCCCTGGCAATGTGAT	0,117	0,026	2,191	**9,9**
X8215	GGUAAUC(C)(C)UGGCAAUGUGAT	0,400	0,051	4,924	**38,6**
X8216	AATCCCTGGCAATGTGAT	0,481	0,113	2,701	**11,5**
X8217	AATCCCTGGCAATGTGAT	0,370	0,357	4,078	**4,2**
X8218	ATCCCTGGCAATGTGAT	0,175	0,110	1,299	**2,1**
X8219	TAAT(C)C(C)TGG(C)AATGTGA	0,110	0,102	1,473	**1,6**
X8220	GGUAAUCCCUGGCAAUGUGAT	5,562	0,255	2,153	**47,0**

Docusign Envelope ID: 7E4C2DFC-1112-4D5D-8C31-F4048EAE7E40

Supp. Table 2. Screening of antimiR conjugate candidates. The sequence for each oligonucleotide used in DM1 TDMs is indicated. The following parameters were calculated: EC_{50}, TC_{50}, E_{max} (maximum fold change), and T_{index} (therapeutic index). The grey row shows the results for our benchmark antimiR-23b (35, 36). Sequence key: N (A, G, T, C): DNA and RNA nucleotides and (C): 5-methyl-2'-O-methyl cytidine.

Name	Sequence (5' > 3')	TC_{50}	EC_{50}	E_{max}	T_{index}
X820	GGUAAUCCCUGGCAAUGUGAU-CHOL	0,857	0,204	7,548	31,70
X82--	GGUAAUCCCUGGCAAUGUGAU	1,704	0,264	1,478	**9,53**
X8200	OLEYL-GGUAAUCCCUGGCAAUGUGAU	4,040	0,010	2,726	**1101,40**
X8201	LINOLEYL-GGUAAUCCCUGGCAAUGUGAU	40,630	0,186	1,835	**400,94**
X8202	TOCOPHEROL-GGUAAUCCCUGGCAAUGUGAU	3,460	0,100	2,211	**76,59**
X8203	CHOLESTEROL-GGUAAUCCCUGGCAAUGUGAU	1,027	1,279	13,654	**10,96**
X8204	PALMITOYL-GGUAAUCCCUGGCAAUGUGAU	2,156	0,460	1,775	**8,32**
X8205	ELAIDOYL-GGUAAUCCCUGGCAAUGUGAU	0,700	1,341	1,628	**0,85**
X8206	STEAROYL -GGUAAUCCCUGGCAAUGUGAU	0,432	0,730	1,848	**1,09**

Supp. Table 3. Leading antimiR candidates selected for further preclinical testing. Sequence key: N (A, G, T, C): DNA and RNA nucleotides and (C): 5-methyl-2'-O-methyl cytidine. The conjugate used in each case is indicated in the table.

Name	Sequence (5' > 3')
X821-7	AT(C)(C)(C)TGG(C)AATGTGA
5'X82107	OLEYL-AT(C)(C)(C)TGG(C)AATGTGA
X82107	AT(C)(C)(C)TGG(C)AATGTGA-OLEYL
X821-8	AT(C)(C)CTGGCAATGTGA
X82108	AT(C)(C)CTGGCAATGTGA-OLEYL
X82148	AT(C)(C)CTGGCAATGTGA-PALITOYL
X831-4	TTAGATCAAGCACAA
X83104	TTAGATCAAGCACAA-OLEYL

Docusign Envelope ID: 7E4C2DFC-1112-4D5D-8C31-F4048EAE7E40

Supp. Table 4. Probes and primers used for RT-qPCR. Sequence key: 6FAM: Fluorescein modification; IAbRQSp: Iowa Black RQ-Sp; MAX: NHS ester modification; BHQ_1: Black Hole Quencher-1.

Gene		Sequence (5'→3')
Mbnl1 (mouse)	**Probe**	/6FAM/TCGCAAATCAGCTGTGAGGAGATTCCCT/IAbRQSp/
	Primer Forward	TACCGATTGCACCACCAAAC
	Primer Reverse	GCTGCTTTCAGCAAAGTTGTC
Mbnl2 (mouse)	**Probe**	/6FAM/CCCGGCAGACAGCACCATGATCGA/IAbRQSp/
	Primer Forward	GAGACAGACTGCCGCTTTG
	Primer Reverse	GGTTACGGTGTTGTCGTTTGT
Gapdh	**Probe**	/MAX/-CGCCTGGTCACCAGGGCTGCT-/BHQ_1/
	Primer Forward	CAACGGATTTGGTCGTATTGG
	Primer Reverse	TGATGGCAACAATATCCACTTTACC